A novel and specific regulator of neuronal V-ATPase in *Drosophila*

Amina Dulac[1], Abdul-Raouf Issa[1,#], Jun Sun[1,§], Giorgio Matassi[2], Baya Chérif-Zahar[1], Daniel Cattaert[3] and Serge Birman[1,*]

[1]Genes Circuits Rhythms and Neuropathology, Brain Plasticity Unit, CNRS, ESPCI Paris, PSL Research University, 10 rue Vauquelin, F-75005 Paris, France

[2]Dipartimento di Scienze Agroalimentari, Ambientali e Animali, University of Udine, Udine, Italy and Université de Picardie Jules Verne, CNRS-UMR 7058 "Ecologie et Dynamique des Systèmes Anthropisés" (EDYSAN), Amiens, France.

[3]INCIA - Institut de Neurosciences Cognitives et Intégratives d'Aquitaine, CNRS, Université de Bordeaux, PAC Talence, allée Geoffroy Saint-Hilaire, F-33615 Pessac cedex, France

*Author for correspondence: serge.birman@espci.fr

[#]*Present address*: Sussex Neuroscience, School of Life Sciences, University of Sussex, Biology Road, Brighton BN1 9QG, UK.

[§]*Present address*: Neurodevelopment Laboratory, School of Biosciences, University of Birmingham, Birmingham B15 2TT, UK.

Abstract

The V-ATPase is a highly conserved enzymatic complex that ensures appropriate levels of acidification in many organelles in virtually all eukaryotic cells. While the general mechanisms of this proton pump have been well studied, little is known about the specific regulations of neuronal V-ATPase. Here, we identify a novel neuronal *Drosophila* protein, named VhaAC45L, predicted from its sequence homology to be part of the V-ATPase family. This protein is addressed to synaptic terminals, and its expression is required for fly development and survival. We observed that VhaAC45L co-immunoprecipitated with V-ATPase subunits and that synaptic vesicles of larval motoneurons were not properly acidified in partial *VhaAC45L* knockdown context. This defect was associated with a decrease in quantal size and locomotor impairments in knockdown animals. Overall, our data provide compelling evidence that VhaAC45L is a specific regulator of neuronal V-ATPase in *Drosophila* that is required for synaptic vesicle acidification and neurotransmitter release.

Key words

ATP6AP1/ATP6AP1L, *Drosophila melanogaster*, neuron, neuromuscular junction, synaptic transmission, synaptic vesicle acidification, V-ATPase complex, VhaAC45L

Introduction

Many cellular processes require a specific electrochemical environment for proper functioning, such as post-translational modifications of proteins in the Golgi apparatus, lysosomal

43 degradation, endosomal ligand-receptor dissociation, or hormone concentration (reviewed in
44 Forgac, 2007). Eukaryotic cells use a highly conserved proton pump, called the vacuolar H^+-
45 ATPase (V-ATPase), to achieve the adequate level of acidity in different cellular compartments
46 (Saroussi and Nelson, 2009). This large enzymatic complex must be tightly regulated, as it is
47 essential for it to be localized on the right membrane, and to fit the different pH ranges specific
48 to each organelle and cell type.
49 In neurons, the V-ATPase plays a crucial role at the synapse, being responsible for acidifying
50 synaptic vesicles and thus providing the driving force for neurotransmitter loading (Moriyama et
51 al., 1992). Recently, neuronal V-ATPase has also gained interest in the context of aging and
52 neurodegenerative diseases, as its dysregulation, and resulting impairment of the autophagy-
53 lysosomal pathway, have been linked to several pathologies such as Alzheimer and Parkinson
54 disease (Colacurcio and Nixon, 2016; Collins and Forgac, 2020). If the core mechanism of the
55 proton pump is now well understood, the regulations conferring the cell-specific functions of
56 neuronal V-ATPase remain largely unknown, considerably limiting its potential use as a
57 therapeutic target.
58 The V-ATPase complex is composed of a cytoplasmic domain (V_1) and a membrane-bound
59 domain (V_0). The V_1 domain contains the catalytic unit responsible for ATP hydrolysis. The
60 energy resulting from this reaction powers a rotational molecular motor spanning from V_1 to V_0,
61 allowing protons to cross membranes through the port contained in V_0 (Vasanthakumar and
62 Rubinstein, 2020). The assembly of V_1 to V_0 is necessary for the pump to function, and
63 reversible dissociation of the two domains has been shown to occur as a way to regulate V-
64 ATPase activity (Collins and Forgac, 2020). Though the core mechanism stays the same, one V-

65 ATPase can differ from another by its composition. In vertebrates, as well as in *Drosophila*, V_0 is
66 made of five subunits (*a*, *c*, *c''*, *d* and *e*), while V_1 contains eight subunits (A, B, C, D, E, F, G and
67 H) (Allan et al., 2005). Each subunit can be coded by several genes, and each gene can produce
68 several isoforms, allowing many different possible combinations to form the full V-ATPase
69 complex. These differences of composition can also have regulatory effects on the complex,
70 both on its localization and on its functional properties (Vasanthakumar and Rubinstein, 2020).
71 The V-ATPase can also be regulated by two accessory subunits, ATP6AP1/Ac45 and
72 ATP6AP2/PRR (Jansen and Martens, 2012). Both proteins are found in the nervous tissue but
73 are also required in other organs, and their mutation has been linked to cognitive impairments
74 as well as systemic symptoms like immunodeficiency or hepatopathy (Jansen et al., 2016;
75 Cannata et al., 2018). These two subunits interact directly with the V_0 domain and are believed
76 to promote assembly of the membrane and soluble regions of the V-ATPase complex (Abbas et
77 al., 2020). Another potential accessory subunit exists in vertebrates, named ATP6AP1-like
78 (ATP6AP1L), which is homologous to ATP6AP1 and has not yet been studied. *Drosophila*
79 possesses identified homologs of ATP6AP1/Ac45 and ATP6AP2/PRR, named VhaAC45 and
80 ATP6AP2, respectively. These proteins also seem to contribute to assembly of the V-ATPase in
81 fly tissues (Schoonderwoert and Martens, 2002-a; Guida et al., 2018).
82 In this study, we examine the localization and function of another still uncharacterized
83 ATP6AP1/Ac45 homolog in *Drosophila*, named VhaAC45L, whose characteristic is to be
84 expressed selectively and ubiquitously in neurons. Whereas a complete deficiency of this
85 protein is lethal, we found that partial *VhaAC45L* knockdown in larval motoneurons impaired
86 synaptic vesicle acidification, leading to reduced quantal size, which is the amplitude of the

87 postsynaptic response to the release of a single synaptic vesicle, and locomotion defects. We
88 also report that VhaAC45L from brain tissue co-immunoprecipitated with V-ATPase subunits,
89 and in particular with ATP6AP2. Overall, our results indicate that VhaAC45L is a novel accessory
90 subunit of the V-ATPase that is specifically involved in the regulation of its activity in neurons.
91

92 ## Results

93 ### VhaAC45L is specifically expressed in neurons and addressed to synaptic areas

94 Here we studied the *Drosophila* gene *CG31030*, identified in FlyBase as a paralog of *VhaAC45*,
95 and so, as another fly ortholog of vertebrate *ATP6AP1/AC45* (Thurmond et al., 2019), that we
96 named therefore *VhaAC45-like (VhaAC45L)*. VhaAC45L and VhaAC45 indeed share 69.9%
97 similarity in amino-acid sequences (Supplementary Figure 1A), and *VhaAC45L* is also classified in
98 the V-ATPase family group by the InterPro database (accession: Q8IMJ0_DROME) (Mitchell et
99 al., 2019). According to FlyAtlas (Chintapalli et al., 2007), *VhaAC45* is apparently expressed
100 rather ubiquitously in *Drosophila* tissues, while in contrast *VhaAC45L* seems to be specifically
101 expressed in the nervous system in both larval and adult flies, making it a possible candidate for
102 the specific regulation of neuronal V-ATPase (Supplementary Figure 1B). To confirm this
103 assumption, we checked by qPCR the repartition of *VhaAC45L* transcripts in three parts of the
104 adult fly body: the head containing the brain, the thorax containing the ventral nerve cord
105 (VNC), and the abdomen, relatively poor in nervous tissue. Both females and males showed
106 highest expression in the head, minor expression in the thorax and no detectable expression in
107 the abdomen (Figure 1A). The expression of *VhaAC45L* therefore closely follows the repartition
108 of the nervous system in the fly body.

109 The single-cell RNA-Seq Scope database (Davie et al., 2018) furthermore indicates that, in
110 *Drosophila*, VhaAC45L is expressed in all neurons, with few or no expression in glial cells. To
111 verify this, we expressed three different *VhaAC45L* RNAi either with the pan-neuronal driver
112 *elav-Gal4* or the pan-glial driver *repo-Gal4* (see Supplementary Table 3 for genotypes of the
113 different *Drosophila* lines used in this study). The expression of *VhaAC45L*^{RNAi1} and *VhaAC45L*^{RNA2}
114 was found to be lethal at embryonic and 1st larval stages, respectively, while *VhaAC45L*^{RNAi3}
115 produced viable adults with a shortened longevity (Supplementary Figure 2), and obvious
116 locomotor impairments. This difference in phenotypes observed with different RNAi constructs
117 could be attributed to a variation in residual levels of the VhaAC45L protein. RT-qPCR
118 experiments showed that the pan-neuronal expression of *VhaAC45L*^{RNAi3} together with the RNAi
119 booster *Dicer-2* (*Dcr-2*) was sufficient to decrease by more than 80% *VhaAC45L* transcripts
120 abundance in extracts from the adult heads (Figure 1B). On the other hand, glial expression of
121 this RNAi construct with *repo-gal4* had no significant effects on *VhaAC45L* transcript level
122 (Figure 1B), confirming that this gene is selectively expressed in neurons. It is interesting to note
123 that both *VhaAC45L*^{RNAi1} and *VhaAC45L*^{RNAi2} also induced lethal phenotypes at various
124 developmental stages when expressed either with a glutamatergic (*VGlut-Gal4*) or a cholinergic
125 (*Cha-Gal4*) driver (data not shown), in accordance with the RNA-Seq data of the Scope website
126 suggesting a pan-neuronal expression of this gene.
127 To validate these observations, we placed the available MIMIC line *VhaAC45L*^{MI107} that contains
128 a stop codon inserted in the middle of the gene (Nagarkar-Jaiswal et al., 2015) over the
129 deficiency *Df(3R)Exel6214* encompassing *VhaAC45L* (Parks et al., 2004). The resulting mutant,
130 likely to be a null, was found to be embryonic lethal, in agreement with the results obtained

131 with two *VhaAC45L* RNAi lines. Remarkably, re-expressing the gene selectively in neurons, using
132 a *UAS-VhaAC45L* construct driven by *elav-Gal4*, was sufficient to rescue this lethality, producing
133 viable and fertile adults with no obvious behavioral defects (Supplementary Table 1). These
134 results strongly indicate that *VhaAC45L* is an essential gene whose expression appears to be
135 specifically required in neurons.
136 Next, we studied the cellular localization of this protein. We used the CRISPR-Cas9 technique to
137 insert a small V5 epitope tag in frame at the 3' end of its gene, disrupting the stop codon, thus
138 generating the *VhaAC45L*^{V5} mutant line (Figure 1C). By immunostaining with a V5-specific
139 antibody, we observed that the general expression pattern of VhaAC45L in adult brain (Figure
140 1D) and larval CNS (Figure 1E) was widespread and similar to that of the synaptic marker
141 Cadherin-N (CadN), indicative of a predominantly synaptic localization. No specific signal was
142 detected in a control w^{1118} line that does not contain the V5-tagged protein (not shown). Some
143 neuronal cell bodies were also marked with the V5 antibody in the *VhaAC45L*^{V5} line, both in
144 adult and larva, and the synapse-containing neuropile areas (like the antennal lobes) were not
145 as sharply defined as with the CadN antibody, suggesting that axons could also be
146 immunopositive. Finally, co-immunostaining of larval body wall muscles with anti-horseradish
147 peroxidase (HRP) antibodies, a marker of *Drosophila* neurons (Jan and Jan, 1982), showed
148 precise co-localization with the V5 signal, indicating that VhaAC45L is addressed to synaptic
149 boutons at the larval neuromuscular junction (Figure 1F).
150
151
152

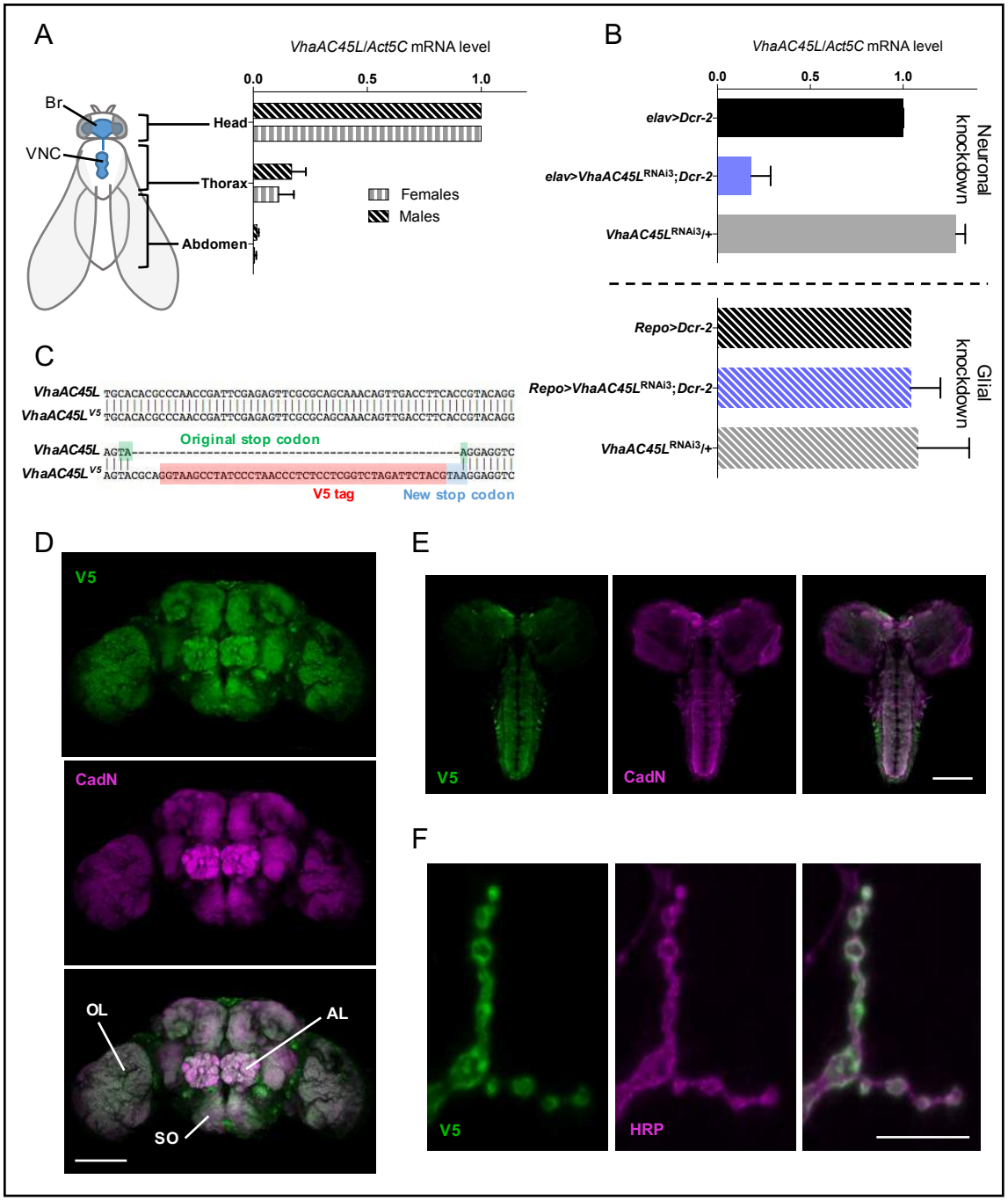

153

154 **Figure 1.** VhaAC45L is expressed in neurons and addressed to synaptic areas. (**A**) In both males and

155 females, *VhaAC45L* mRNA abundance follows the localization of the CNS (shown in blue on the fly

156 sketch), with the highest expression in the head. Br: brain, VNC: ventral nerve cord. Results of three

157 independent experiments. (**B**) Expression of *VhaAC45L*^{RNAi3} with *Dcr-2* in all neurons using *elav-Gal4*

158 decreased *VhaAC45L* mRNA level in head by more than 80%, while expression of the RNAi construct and

159 Dcr-2 in all adult glial cells with *repo-Gal4* had not effect. Results of three independent experiments.
160 Mean values with SD are reported on the graphs. (**C**) Construction of the *VhaAC45L*^{V5} mutant strain. A V5
161 tag (in red) was fused to the C-terminal end of the VhaAC45L protein by inserting the V5 coding
162 sequence ended by a new stop codon (in blue) in place of the original stop codon (in green) in the
163 *VhaAC45L* gene using the CRISPR-Cas9 technology. (**D, E**) Anti-V5 immunostaining in the *VhaAC45L*^{V5}
164 strain revealed that VhaAC45L is mainly addressed to synaptic areas in the adult brain (**D**) and larval CNS
165 (**E**), as indicated by its apparent colocalization with the presynaptic marker Cadherin-N (CadN). OL: optic
166 lobe, AL: antennal lobe, SO: subœsophageal ganglion. (**F**) A V5-immunopositive signal was also detected
167 at the neuromuscular junction of *VhaAC45L*^{V5} larvae, and found to co-localize with anti-horseradish
168 peroxidase (HRP) immunostaining that labels neuronal membranes, confirming the synaptic localization
169 of *VhaAC45L*. Scale bars: 100 µm in D and E, and 10 µm in F.
170

171 **VhaAC45L co-immunoprecipitates with V-ATPase proteins**

172 The VhaAC45L protein is predicted to be part of the InterPro V-ATPase family, but no
173 experimental information is currently available regarding its potential interactors. To determine
174 whether VhaAC45L could interact, directly or indirectly, with subunits of the V-ATPase complex,
175 we carried out co-immunoprecipitation experiments using an anti-V5 antibody on proteins
176 extracted from heads of *VhaAC45L*^{V5} mutants and *w*^{1118} control flies, followed by nano LC-MS/MS
177 mass-spectrometry analysis of the precipitated proteins. Three independent experiments were
178 performed to increase reliability, and in total, 410 proteins were identified in all three
179 experiments. Among those, only 12 proteins had at least a two-fold abundance difference with
180 the control in all three experiments (Figure 2A and Supplementary Table 2), one of them being,
181 as expected, the co-immunoprecipitation target VhaAC45L. Remarkably, three of the 11 other

182 proteins were identified as subunits of the V-ATPase complex: Vha100-1, VhaAC39-1 and
183 ATP6AP2 (Figure 2B).
184 *Vha100-1* and *VhaAC39-1* code for subunits *a* and *d* of the V_0 domain, respectively
185 (Vasanthakumar and Rubinstein, 2020). The subunit *a*, coded by five different genes in
186 *Drosophila*, is the proton port of the pump (Collins and Forgac, 2020). Among the five isoforms,
187 Vha100-1, which co-immunoprecipitated with VhaAC45L in our experiments, has been shown to
188 be specifically required in neurons and present at the synapse (Hiesenger et al., 2005). Subunit *d*
189 of V_0 is coded by two *Drosophila* genes: *VhaAC39-1* and *VhaAC39-2*, and only the first co-
190 immunoprecipitated with VhaAC45L. According to FlyAtlas, VhaAC39-1 is expressed in many
191 tissues and enriched in the brain, while VhaAC39-2 seems to be mostly found in testis and
192 salivary glands. For both V_0 subunits, VhaAC45L thus co-precipitated with the likely neuronal
193 isoform. The co-immunoprecipitated V-ATPase subunit which appeared to be the most enriched
194 in the *VhaAC45L*^{V5} sample was interestingly the accessory subunit ATP6AP2, suggesting a possible
195 direct interaction between this protein and VhaAC45L (Supplementary Table 2). These
196 experiments therefore reinforce the hypothesis that VhaAC45L directly interacts with the
197 neuronal V-ATPase complex, and more specifically with V_0 since all detected partners belong, or
198 interact, with this domain.
199

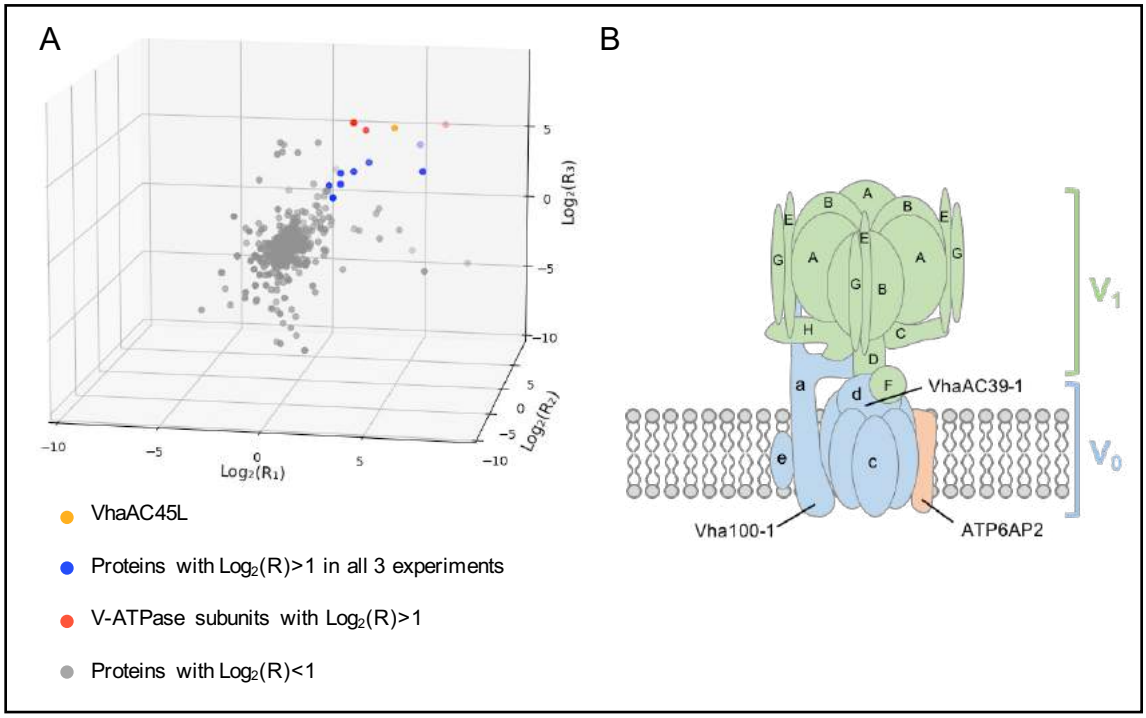

200

201 **Figure 2.** VhaAC45L co-immunoprecipitates with V-ATPase subunits. (**A**) Scatter plot of proteins
202 identified by nano LC-MS/MS in three independent co-immunoprecipitation experiments using anti-V5
203 antibodies. R_1 and R_2 represent the abundance ratio of proteins identified in adult head extracts from
204 *VhaAC45L*^{V5} over *w*^{1118} control in experiments 1 and 2, respectively. Solid lines indicate $Log_2(R) = 1$, which
205 corresponds to a two-fold abundance difference. 12 proteins were found to be at least twice as
206 abundant in *VhaAC45L*^{V5} as in the control in all three experiments (red or blue dots on the graph). One of
207 them is the immunoprecipitation target VhaAC45L (yellow dot) and three of these proteins belong to the
208 V-ATPase complex (red dots). A list of these 12 proteins with their $Log_2(R)$ values is provided in
209 Supplementary Table 2. (**B**) Standard model of the *Drosophila* V-ATPase complex showing structure of
210 the V1 and V0 domains and the predicted localization of the three subunits that co-immunoprecipitated
211 with VhaAC45L.

212

213

214 **VhaAC45L knockdown increases the pH of synaptic vesicles**

215 Because VhaAC45L appeared to be mainly localized in synaptic areas (see Figure 1), we chose to
216 look at the physiological effect of its disruption at the *Drosophila* larval neuromuscular junction,
217 a model that has contributed to the study of many synaptic processes. At synaptic nerve
218 endings, a prominent role of the V-ATPase is to acidify the lumen of synaptic vesicles, the
219 electrochemical gradient generated providing the driving force to load and concentrate the
220 neurotransmitters. Thus, a malfunction of synaptic V-ATPase should induce a decrease of
221 neurotransmitter concentration inside the vesicles, potentially resulting in an altered synaptic
222 transmission.

223 To test this hypothesis, we co-expressed each of the two strongest *VhaAC45L* RNAi constructs
224 together with VMAT-pHluorin, a pH-sensitive probe targeted to synaptic vesicles (Wu et al.,
225 2013), in larval motoneurons using the glutamatergic driver *OK371-Gal4.* Both RNAi1 and RNAi2
226 induced a lethal phenotype at pupal stage in these conditions. VMAT-pHluorin is an ecliptic
227 pHluorin that is fluorescent at neutral pH, and gets quenched, by protonation, at acidic pH
228 (Miesenböck et al., 1998). Thus, in control condition, VMAT-pHluorin should not be fluorescent
229 in synaptic vesicles, whose pH is at around 5.5, but only when externalized on the presynaptic
230 membrane during exocytosis, and so, in contact with the more neutral synaptic cleft milieu. In
231 the case of an acidification defect of synaptic vesicles, the probe could be fluorescent both in
232 synaptic vesicles, where pH would be abnormally high, and on the presynaptic membrane
233 (Figure 3A, central panel).

234 In order to evaluate the ratio of the internal fluorescence (from synaptic vesicles) over the
235 external fluorescence (from the presynaptic membrane) at the neuromuscular junction of

236 *VhaAC45L* knockdown larvae compared to controls, we first quenched the external signal by
237 replacing the physiological milieu by an identical one with pH adjusted to 5.5 (Figure 3A, left
238 panel). This operation resulted in only the internal signal being conserved. In controls, this
239 meant that all signal was abolished, as expected because the synaptic vesicles were normally
240 acidified (Figure 3B, left panel). In contrast and strikingly, a residual signal was still visible in this
241 acidic milieu in both RNAi1 and RNAi2 knockdown larvae (Figure 3B, right panel). Quantification
242 of the ratio of fluorescence area in acidic milieu over neutral milieu showed that about 37% of
243 the total signal remained visible in the RNAi larvae after external quenching (Figure 3C and D).
244 To verify that the residual signal seen in knockdown larvae was indeed coming from inside
245 vesicles, the opposite strategy was used: instead of quenching the outside signal, we revealed
246 all the internal one by collapsing the pH gradient of synaptic vesicles (Figure 3A, right panel). To
247 do so, we replaced the physiological milieu by an ammonium solution, as previously described
248 (Poskanzer and Davis, 2004). This solution had the same composition except that 50 mM NaCl
249 were replaced by 50 mM NH_4Cl. Ammonium and ammonia being in equilibrium ($NH_4^+ \rightleftarrows NH_3 +$
250 H^+), uncharged ammonia crosses membranes and binds to protons leading to an alkalization of
251 vesicle lumen pH. This increase of vesicular pH is maintained during NH_4Cl exposure. In control
252 condition, this gradient collapse should reveal the VMAT-pHluorin probe present in synaptic
253 vesicles and thus highly increase the fluorescent signal. On the contrary, in the case of an
254 acidification defect, the signal should remain fairly stable since synaptic vesicles are already
255 fluorescent. Results were consistent with this hypothesis: while the fluorescence of controls
256 increased about 3 folds in the pH collapsing ammonium solution, the signal in *VhaAC45L*
257 knockdown larvae hardly rose by 10 to 20% depending on the RNAi construct (Figure 3E, F and

258 G). Taken together, these results indicate that *VhaAC45L* knockdown significantly decreases

259 protons concentration in synaptic vesicles of motoneuron terminals.

260

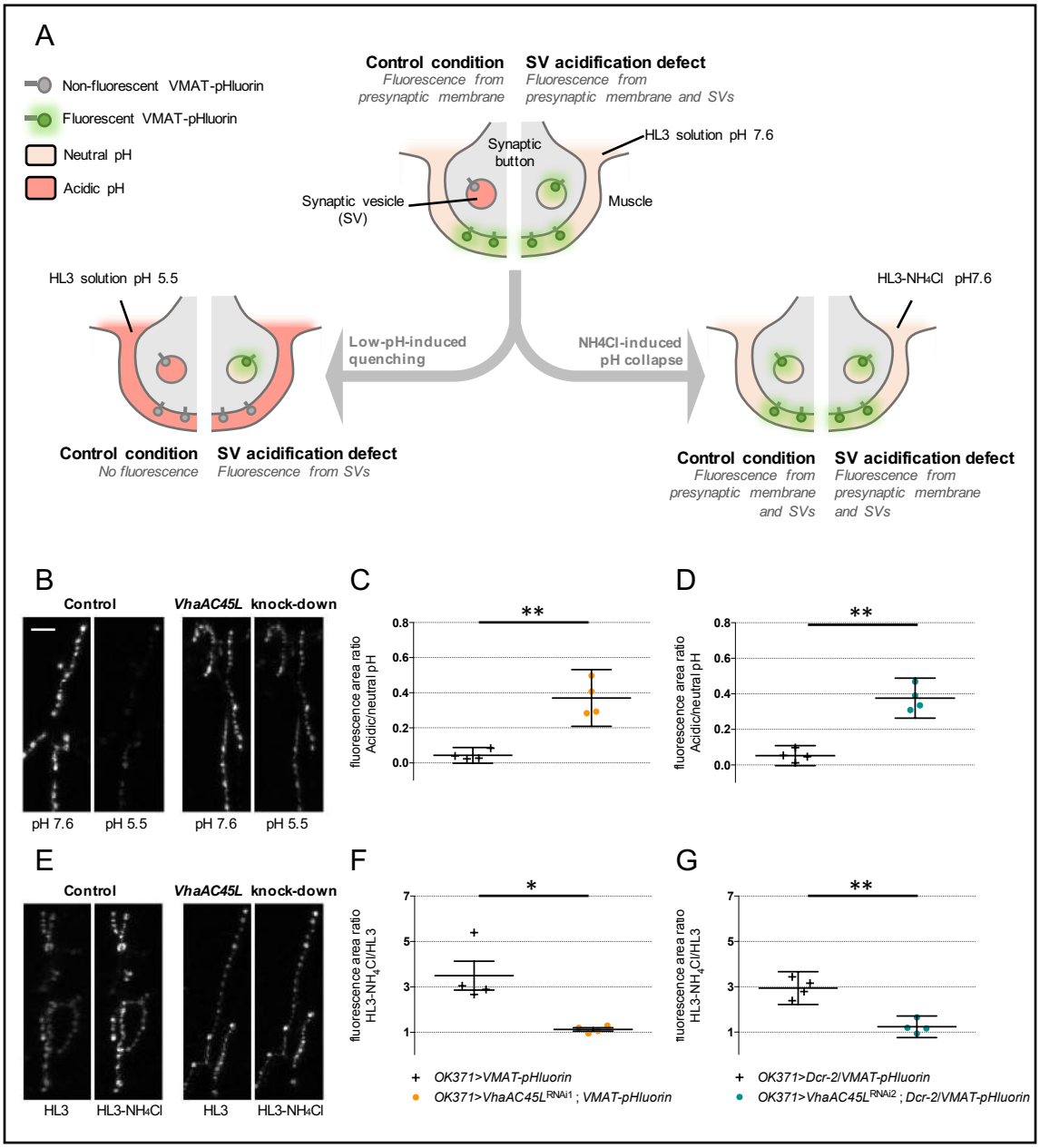

261

262 **Figure 3.** VhaAC45L knockdown larvae have a synaptic vesicle acidification defect. (**A**) Schematic

263 representation of the protocols used to assess relative acidity levels of synaptic vesicles at the larval

264 neuromuscular junction. (*Top center diagram*) In control conditions, fluorescence can be emitted by

265 VMAT-pHluorin in the presynaptic membrane but not in synaptic vesicles since their lumen is acidified. In
266 case of defective synaptic vesicle acidification, both the presynaptic membrane and synaptic vesicles
267 should emit fluorescence. (*Left diagram*) The fluorescence emitted by VMAT-pHluorin in the presynaptic
268 membrane can be quenched by replacing the extracellular medium with an acidic HL3 solution. This
269 quenching should result in an almost complete extinction of the signal in control flies, in which synaptic
270 vesicles are normally acidified, while a residual signal is expected to be visible in flies having a synaptic
271 vesicle acidification defect. (*Right diagram*) Replacement of 50 mM NaCl by 50 mM NH_4Cl in the neutral
272 HL3 solution should lead to a collapse of the pH gradients due to the free diffusion of NH3 in
273 membranes, so that fluorescence will be emitted both by the presynaptic membrane and synaptic
274 vesicles both in control and mutant conditions. (**B**) Representative pictures showing the effect of
275 perfusing an acidic HL3 solution on VMAT-pHluorin fluorescence in control and *VhaAC45L* knockdown
276 larvae. (**C**, **D**) Quantification of the ratio of the fluorescence level at pH 5.5 over the original signal at pH
277 7.6. Whereas the low pH extinguished fluorescence in control flies, about 37% of the signal persisted
278 after quenching in *VhaAC45L* knockdown larvae using two different RNAi constructs. (**E**) Representative
279 pictures showing the effect of collapsing the synaptic vesicle pH by perfusing HL3-NH_4Cl in control and
280 *VhaAC45L* knockdown larvae. (**F**, **G**) Quantification of the ratio of the signal in HL3-NH_4Cl over the
281 original signal in HL3 showed that fluorescence increased about 3-fold in controls while it only rose by 10
282 to 20% depending on the RNAi in *VhaAC45L* knockdown larvae. Results of four independent
283 experiments, with 3-5 larvae analyzed per genotype in each experiment. Paired Student's *t*-test, $*p <$
284 0.05 $**p < 0.01$. Mean values with 95% confidence intervals are reported on the graphs. Scale bar: 15 μm
285 in B and E.
286
287
288

289 **VhaAC45L downregulation decreases larval locomotor performance**

290 A reduced pH gradient of synaptic vesicles in larval motoneurons could alter synaptic
291 transmission and, consequently, the larval locomotor behavior. To assess locomotion, we
292 recorded the spontaneous crawling of 3rd-instar larvae expressing *VhaAC45L* RNAi1 or RNAi2 in
293 motoneurons with *OK371-Gal4* on an agar plate with no food source for 2-min periods. Tracking
294 was then performed using the FIMtrack software (Risse et al., 2014), allowing measurement of
295 the total distance travelled and of the stride size, defined as the distance crawled during one
296 peristaltic wave of muscle contraction, and duration (Figure 4A). The knockdown larvae
297 obviously moved less than controls on the plate, as confirmed by their trajectory maps (Figure
298 4B and C), travelling a distance only half as long as controls with both RNAi (Figure 4E and F).
299 This effect was not simply due to a difference in larval size, as the average length and width of
300 recorded larvae were not significantly different (Supplementary Figure 3).
301 In contrast, the stride size actually showed little or no difference, depending on the RNAi,
302 between knockdown larvae and controls (Figure 4G and H). Instead, we found that the stride
303 duration, which is the time necessary to accomplish one peristaltic wave, was significantly
304 longer in knockdown animals compared to controls for both RNAi (Figure 4I and J). These results
305 suggest that the knockdown larvae may need about twice as much time as controls to reach the
306 required level of muscular contraction to accomplish one stride. This could be a compensatory
307 mechanism to adapt to a lower amount of neurotransmitter released in response to motor
308 nerve stimulation, as would be expected if synaptic vesicles are less filled with neurotransmitter
309 in *VhaAC45L* knockdown context.
310

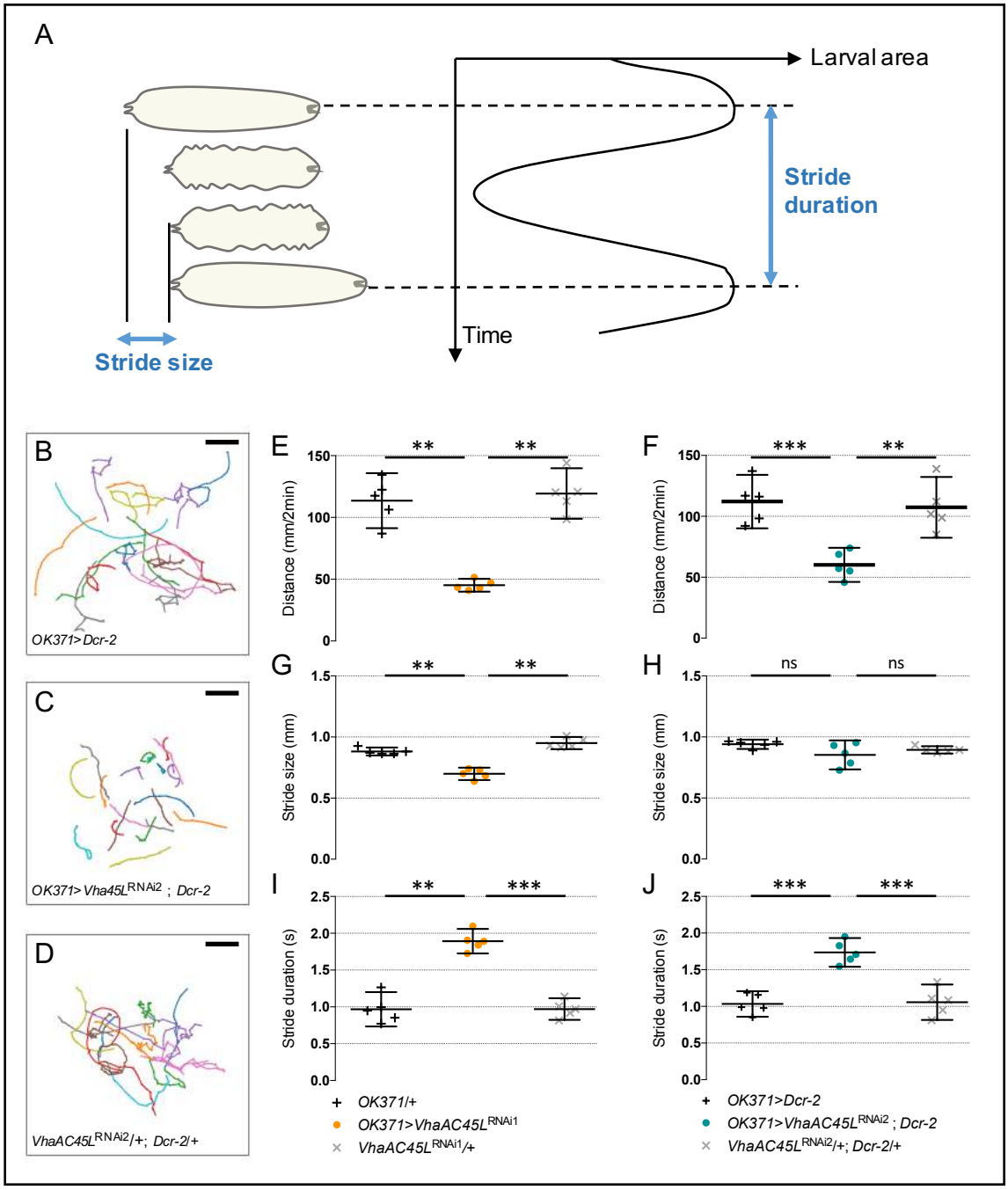

Figure 4. VhaAC45L downregulation in motoneurons decreases larval locomotor performance. (**A**) Schematic representation of the successive phases of larval locomotion. Stride size is defined as the distance crawled during one peristaltic wave of muscle contraction, while stride duration is the time necessary for the completion of one peristaltic wave. (**B**-**D**) Locomotor trails of individual larvae recorded over a period of 2 min. Larvae expressing *VhaAC45L* RNAi in motoneurons show reduced spontaneous

317 movements (**C**) compared to the driver and UAS controls (**B** and **D**, respectively). Scale bar: 25 mm. (**E**, **F**)
318 Quantification of the travelled distances confirmed that knocking down *VhaAC45L* in motoneurons with
319 two different RNAi induced significant locomotor defects. (**G**-**J**) Stride size (**G**, **H**) appears to be much less
320 affected than stride duration (**I**, **J**) in the knocked-down larvae. Result of five independent experiments,
321 with 3-4 larvae analyzed per genotype in each experiment. Repeated-measures one-way ANOVA with
322 Dunnett's post-test for multiple comparisons, $^{**}p < 0.01$, $^{***}p < 0{,}001$. Mean values with 95%
323 confidence intervals are reported on the graphs.
324

325 **Quantal size is reduced in *VhaAC45L* knockdown larvae**

326 The locomotor deficit of *VhaAC45L* knockdown larvae could originate from an impairment of
327 synaptic transmission at the neuromuscular junction or a defect in the central control of motor
328 behavior, or both. To determine if neurotransmission was affected, we carried out
329 electrophysiological recordings to measure the quantal size, which is the postsynaptic response
330 to the release of one synaptic vesicle, at the larval neuromuscular junction. We expressed
331 *VhaAC45L* RNAi1 or RNAi2 in motoneurons with the *OK371-Gal4* driver, and recorded
332 spontaneous miniature excitatory postsynaptic potentials (mEPSPs) intracellularly from ventral
333 longitudinal abdominal muscle 6 of segment A3 (Figure 5A). These muscles are innervated by
334 synaptic boutons that are clearly marked by *OK371-Gal4*, as shown by the co-localization of
335 membrane-associated GFP and the postsynaptic marker Discs large (Dlg) in *OK371>mCD8::GFP*
336 flies (Figure 5B). Representative amplitude distributions of mEPSPs in a control and RNAi1 larvae are
337 shown in Figure 5C. Quantal analysis of recorded events confirmed that both RNAi1 and RNAi2
338 knockdown larvae have a significantly reduced quantal size compared to controls (Figure 5D),
339 suggesting a decrease in glutamate vesicular uptake, and potentially linking vesicle acidification

340 defect and locomotor impairment. The V-ATPase dysfunction in synapses of *VhaAC45L*
341 knockdown larvae apparently led to incomplete loading of vesicles, thus decreasing the amount
342 of neurotransmitter released per unit of time during a peristaltic wave, and therefore slowing
343 down larval locomotion. Although the mean frequency of mEPSPs of both RNAi1 and RNAi2
344 larvae appeared lower than controls, this effect was not statistically significant (Figure 5E). This
345 may suggest that the acidification defect induced by *VhaAC45L* RNAi knockdown did not highly
346 increased the number of empty vesicles.
347

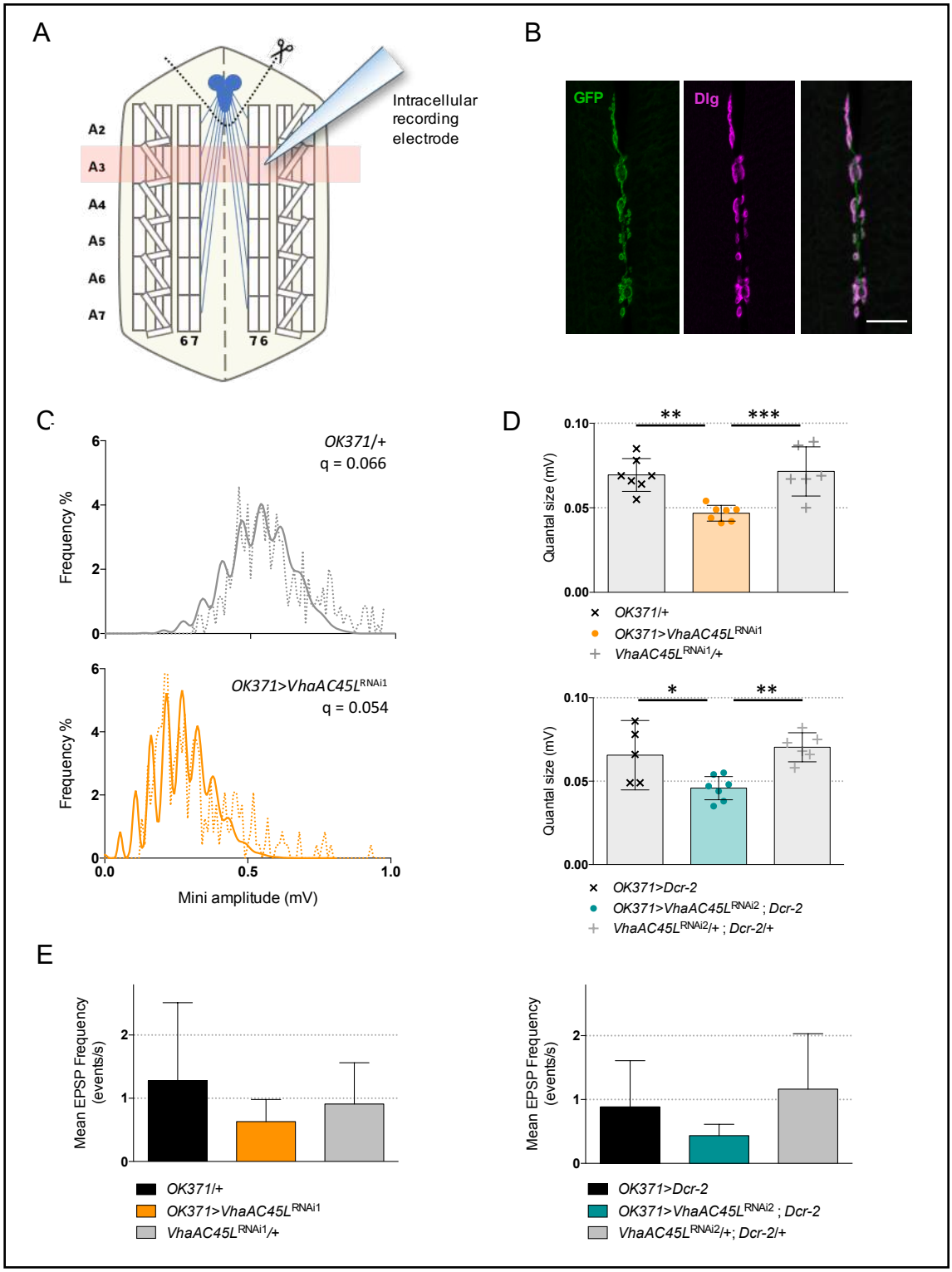

348

349 **Figure 5.** Synaptic quanta size is reduced in *VhaAC45L* knockdown larvae. (**A**) Schematic representation

350 of a dissected larval fillet. Spontaneous excitatory postsynaptic potentials (EPSPs) were recorded

351 intracellularly from the ventral longitudinal abdominal muscle 6 in segment A3. (**B**) Expression of
352 membrane-associated mCD8::GFP with the glutamatergic driver *OK371-Gal4* strongly labels the
353 presynaptic nerve endings at the neuromuscular junction of muscles 6-7 in segment A3. The scaffolding
354 protein Discs large (Dlg) was used as a postsynaptic marker. Scale bar: 20 μm. (**C**) Representative
355 distributions of spontaneous mEPSPs recorded in a control larva (*top panel*, *in grey*) and a *VhaAC45L*
356 RNAi knockdown larva (*bottom panel, in orange*). The dotted lines represent actually recorded
357 amplitudes and the plain lines the computed theoretical distributions. Genotypes and quantal size (q)
358 are indicated on each graph. (**D**) Quantal analysis of recorded events showed that knockdown larvae
359 have a significantly reduced synaptic quanta size compared to controls, both with *VhaAC45L* RNAi1 (*top*
360 *panel, in orange)* or RNAi2 (*bottom panel*, *in blue*). (E) Although both RNAi1 (*left panel*) and RNAi2 (*right*
361 *panel*) larvae had a lower mean EPSP frequency than controls, this difference was not statistically
362 significant. One-way ANOVA with Dunnett's post-test for multiple comparisons, *$p < 0.05$, **$p < 0.01$,
363 ***$p < 0.001$. Mean values with 95% confidence intervals are reported on the graphs.
364
365

366 ## Discussion

367 In this study, we have investigated the hypothesis that a previously uncharacterized *Drosophila*
368 protein, called VhaAC45L, is a regulator of the neuronal V-ATPase. At variance with its broadly
369 expressed paralog VhaAC45, we have shown that VhaAC45L is found mainly, if not only, in
370 neurons. We also provide evidence that VhaAC45L interacts with two constitutive subunits and
371 one accessory subunit of the V-ATPase, the constitutive ones being also enriched in neurons,
372 and that it is required to have properly acidified synaptic vesicles. This implies that VhaAC45L is
373 an essential protein for nervous system functioning in *Drosophila*.

374 In yeast, all V-ATPase subunits are coded by a single gene, with the exception of the V_0 subunit
375 *a*. The knock-out of any of the single-gene subunits all present a similar phenotype: the inability
376 to survive in a neutral pH environment (Nelson, 2003). For subunit *a*, the same phenotype was
377 only achieved in a double-mutant of both isoforms (Manolson et al., 1994). In multicellular
378 organisms, mutations of V-ATPase subunits, or accessory proteins, also often lead to a lethal
379 phenotype at various developmental stages, whether in mice (Inoue et al., 1999; Sun-Wada et
380 al., 2000; Schoonderwoert et al., 2002-b), *C. elegans* (Lee et al., 2010), or flies (Davies et al.,
381 1996; Allan et al., 2005). Similarly, a *VhaAC45L* null mutant was found to be embryonic lethal,
382 and, interestingly, this lethality could be rescued to the adult stage by re-expressing *VhaAC45L*
383 in all neurons, showing that the protein is specifically required in this cell type for fly survival.
384 The percentage of adult survivors was about three times less than what would be expected in
385 case of a full rescue (Supplementary Table 1) and the missing two-thirds likely died at an early
386 developmental stage as no larval lethality was observed. This could be explained by the fact that
387 VhaAC45L protein re-expression in rescued knock-out flies first required the expression of Gal4
388 under regulation of the *elav* promoter, which starts to express rather late in embryos, followed
389 by activation of the UAS sequence upstream the *VhaAC45L* insert. So, it is possible that part of
390 the mutant embryos did not survive the delay inherent to this ectopic expression process.
391 We found that *VhaAC45L* transcripts follows the repartition of the nervous system, being mainly
392 found in *Drosophila* head. Moreover, pan-neuronal expression of $VhaAC45L^{RNAi3}$, the RNAi
393 construct with the weakest effect on fly survival, was sufficient to decrease by more than 80%
394 its level in the head of adult escapers. These results indicate that VhaAC45L expression is mainly
395 neuronal, if not even entirely restricted to neurons. In addition, VhaAC45L cellular localization

396 shows similarity with a synaptic pattern. Cell bodies were also marked, although generally less
397 strongly. Synaptic protein complexes can be assembled in the cell bodies before being
398 transported in axons, and it is the case for the soluble and membrane-bound domains of
399 synaptic V-ATPase, as was shown in *Torpedo* (Morel et al., 1998). It is difficult to decide whether
400 the signal coming from cell bodies corresponds to a functional site for VhaAC45L or rather to
401 newly produced proteins that have not yet been targeted to synapses. However, the prominent
402 signal in synaptic areas led us to assume that VhaAC45L plays an important role in some
403 synaptic processes.
404 In presynaptic terminals, the most abundant organelles are synaptic vesicles, which require
405 acidification to provide the driving force for neurotransmitter loading. This acidification is
406 ensured by the V-ATPase pump, which generates an electrochemical gradient by importing
407 protons into the vesicle lumen, thus creating both a membrane potential ($\Delta\Psi$, inside positive
408 voltage) and a pH gradient (ΔpH, acidic lumen). Our experiments showed that the knockdown of
409 *VhaAC45L* at the glutamatergic larval neuromuscular junction increased the internal pH of
410 synaptic vesicles, and so decreased the ΔpH component of the electrochemical gradient
411 generated by the V-ATPase. This result is however by itself insufficient to conclude to a
412 dysfunction of the proton pump, since other players have been shown to influence synaptic
413 vesicle pH gradient downstream V-ATPase activity. For example, cation/H^+ exchangers, found on
414 synaptic vesicles, can decrease ΔpH while increasing $\Delta\Psi$ by exchanging cations, like Na^+ or K^+,
415 against luminal H^+ (Takamori, 2016). This activity can be upregulated by increased intracellular
416 concentration of these cations (Huang and Trussell, 2014). Glutamate being negatively charged,
417 its transport across vesicular membrane is predominantly driven by $\Delta\Psi$ (Maycox et al., 1988;

418 Tabb at al., 1992). As a consequence, the increased membrane potential resulting from up-
419 regulation of cation/H+ exchangers actually facilitates glutamate uptake (Goh et al., 2011;
420 Huang and Trussell, 2014). We measured synaptic quanta size by quantal analysis of mEPSPs of
421 *VhaAC45L* knockdown larvae and found that it was decreased, contrary to what would be
422 expected in the case of an upregulation of cation/H^+ exchanger activity. This apparent decrease
423 of vesicular glutamate concentration was corroborated by its phenotypical consequence,
424 namely the locomotion defect exhibited by knockdown larvae. This suggests that the observed
425 diminution of ΔpH is correlated with a diminution of $\Delta\Psi$, thus pointing towards a V-ATPase
426 malfunction. This hypothesis is further supported by the co-immunoprecipitation of VhaAC45L
427 with three V-ATPase subunits, with all of them being associated with the neuronal V-ATPase.
428 Altogether, these results strongly suggest that VhaAC45L is a neuronal protein necessary to V-
429 ATPase function in synapses. Some V-ATPase subunits isoforms have been shown to target
430 specific subcellular compartments, like the *Torpedo* V_0 a1 isoform which is found in synaptic V-
431 ATPase and not in neuronal cell bodies (Morel et al., 2003). Similarly, VhaAC45L could be
432 specifically involved in the regulation of synaptic V-ATPase, or, alternatively, globally act on all
433 neuronal V-ATPase. Specificity level could even be pushed further, since synaptic vesicles are
434 not the only organelles requiring acidification that are localized in synapses. Thus, a synaptic V-
435 ATPase regulator could be devoted to synaptic vesicles as it could be affecting more generally all
436 synaptic V-ATPase complexes, indifferently of their membrane localization. The answer to such
437 questions could help better understand regulations of synaptic transmission, since synaptic V-
438 ATPase activity is one of the pre-synaptic modulators of quantal response (Takamori, 2016;
439 Gowrisankaran and Milosevic, 2020).

440 While accessory subunits directly interact with V-ATPase domains, other stimulus can indirectly
441 affect activity of the complex, like glucose concentration or serotonin (Sautin et al., 2005; Voss
442 et al., 2007). Co-precipitation of VhaAC45L with V-ATPase subunits does not necessarily imply a
443 direct interaction, but suggests *a minima* an indirect association with the complex, possibly in a
444 non-transient manner. The impairment in V-ATPase activity induced by VhaAC45L
445 downregulation rules out the hypothesis of an inhibitory action of this protein on the proton
446 pump. Nevertheless, the precise requirement of VhaAC45L for activity of the V-ATPase complex
447 still remains unknown to date. Lethality of the mutant could indicate an essential role of
448 VhaAC45L in V-ATPase function. However, some V-ATPase regulators and accessory subunits
449 have been found in other signaling pathways, like ATP6AP2 in the renin-angiotensin system
450 (Nguyen, 2010), so we cannot exclude that lethality could be due to VhaAC45L playing a part in
451 other vital neuronal functions. High signal in axons could also point to a role in targeting the
452 complex to the synapses. The two domains of the V-ATPase, V0 and V1, are believed to be
453 assembled in cellular bodies before being separately transported to synaptic area, V_0 by fast
454 axonal anterograde transport, most likely directly on new synaptic vesicles, and V_1 by slow
455 axonal transport like other cytoplasmic synaptic proteins (Morel et al., 1998). VhaAC45L could
456 be involved in the transport of one of the two domains, and effects of VhaAC45L knockdown
457 could then result from a decreased synaptic abundance of the affected V-ATPase domain.
458 However, it is believed that only one copy of the V-ATPase complex is sufficient to properly
459 acidify one synaptic vesicle (Takamori et al., 2006), a consequence of this being that
460 neurotransmitter loading would be an all-or-none process. Consistent with this, mutation of the
461 *Drosophila* synaptic V_0 subunit Vha100-1 does not seem to impact quantal size but rather

462 mEPSP frequency, potentially reflecting the presence of an increased number of empty synaptic
463 vesicles (Hiesinger et al., 2005). Similarly, a reduction in the frequency of spontaneous quantal
464 events with no change in quantal size was observed when the *Drosophila* vesicular
465 glutamatergic transporter (VGlut) was downregulated, also suggesting that a single copy of
466 VGlut is sufficient for proper acidification of a vesicle (Daniels et al., 2006). The fact that
467 VhaAC45L knockdown changes the quantal size but not significantly mEPSP frequency seems to
468 point toward a role of this accessory protein in V-ATPase efficiency, rather than in a process
469 affecting the abundance of the complex such as synaptic targeting.
470 In this respect, it is interesting to note that the V-ATPase protein that more consistently co-
471 immunoprecipitated with VhaAC45L in our experiments is the accessory subunit ATP6AP2, the
472 fly homolog of human ATP6AP2/PRR. Together with ATP6AP1/Ac45, ATP6AP2 has been
473 proposed to enable the assembly and disassembly of the catalytic and membrane domains of
474 the V-ATPase in the mammalian brain (Abbas et al., 2020). This suggests that VhaAC45L could
475 play a role in the regulation of these dynamic processes, which could also influence
476 neurotransmitter loading and release in a more continuous way. Our results suggest indeed that
477 modulating V-ATPase activity in presynaptic terminals can finely affect quantal size. Whether
478 such regulation actually occurs in physiological, or pathological, conditions remains to be
479 established. Importantly, human *ATP6AP2*/*PRR* is known to be a Parkinsonism candidate gene
480 and its mutations in humans, mice or flies can lead to cognitive impairment, neurodegeneration
481 and epilepsy (Korvatska et al., 2013; Dubos et al. 2015; Ichihara and Yatabe, 2019). It is
482 therefore of major interest to identify a potential new interactor of ATP6AP2 that is specific to
483 the nervous system, as it could help better understand the consequences of V-ATPase

484 dysregulation on synaptic transmission in pathological contexts. Accordingly, it would be very
485 interesting to determine whether human ATP6AP1 and/or ATP6AP1L share a conserved
486 function with *Drosophila* VhaAC45L in the nervous system. Every new actor identified allows us
487 to paint a more detailed picture of the complex regulations surrounding neuronal V-ATPase
488 specificity, providing new angles for potential therapeutic targets, and a better understanding of
489 fundamental processes such as synaptic transmission.
490
491

492 ## Materials and methods

493

494 ### *Drosophila* strains, construction and culture

495 Flies were raised on standard agar-cornmeal-yeast medium, at 25°C in a 12:12h light-dark cycle.
496 *VhaAC45L* RNAi strains and mutants were obtained from the Bloomington *Drosophila* stock
497 center (BDSC) and the Vienna Drosophila Resource Center (VDRC). Detailed genotypes and
498 references of these lines are provided in Supplementary Table 3. To construct the *UAS-*
499 *VhaAC45L* strain, the *VhaAC45L* cDNA was PCR amplified from the clone RH09162 obtained
500 from the *Drosophila* Genomics Resource Center, Indiana University, USA, using the following
501 primers with added restriction sites: P1-EcoRI (forward) 5'-
502 CCATCCGAATTCAAAATGCAGCTGATTCTCGT and P2-XhoI (reverse) 5'-
503 TGGCTGCTCGAGATCTATTGGGTTATGAGAGA. The 1160 bp PCR fragment was inserted into
504 pUAST (Brand and Perrimon, 1993), verified by sequencing (GATC Biotech) and sent to
505 BestGene, Chino Hills, CA, USA, for P-element transformation by random insertion in w^{1118}

506 background. A 2d-chromosome insertion of *UAS-VhaAC45L* that yielded strong expression of the
507 transgene was used thereafter.
508
509 **Reverse transcription-coupled qPCR**
510 Total RNAs were extracted from 20 heads (or 15 thoraces or 15 abdomens) of 8-day-old flies
511 using the QIAzol Lysis reagent (Qiagen). The Maxima First Strand cDNA Synthesis Kit (Thermo
512 Fisher Scientific, ref. K1671) was used with oligo(dT)20 primers to synthesize the cDNAs.
513 Relative quantitative PCR assays were carried out using a LightCycler 480 and the SYBR Green I
514 Master mix (Roche LifeScience), with *Act5C* as internal control for normalization of mRNA levels.
515 All reactions were performed in triplicate. The specificity of amplification products was assessed
516 by melting curve analyses. The following forward and reverse primers, were used: for
517 *VhaAC45L*, 5'-GGCTTCGTTGTAGGCCAACAGA and 5'-CACCAGGTATCCCAAGTTCCAGA; for *Act5C*,
518 5'-CGTCGACCATGAAGATCAAG and 5'-TTGGAGATCCACATCTGCTG.
519
520 **CRISPR/Ca9 gene tagging**
521 The sequence of a V5 tag was inserted in frame after the coding sequence of the *VhaAC45L*
522 gene, using a homology-directed repair CRISPR-Cas9 method (see Figure 1C). The following
523 guide RNA sequence: 5'-TTCACCGTACAGGAGTAAGG-3' was cloned into the BbsI site of pCFD3:
524 U6:3-gRNA plasmid (Port et al., 2014) (kind gift of Hervé Tricoire, Université de Paris, Paris,
525 France). This plasmid was then injected, at a concentration of 500 ng/μL, with the following
526 single-stranded oligodeoxynucleotide (ssODN) donor repair template: 5'-
527 GTTCGCGCAGCAAACAGTTGACCTTCACCGTACAGGAGTACGCAGGTAAGCCTATCCCTAACCCTCTCCT

528 CGGTCTAGATTCTACGTAAGGAGGTCATAAGTCTCTGATGAACCAATAGATCTCGGGC-3' (synthetized
529 by Integrated DNA Technology, Leuven, Belgium), also at a concentration of 500 ng/μL (the
530 sequence underlined corresponds to the in-frame V5 tag), into *nos-cas9* embryos (genotype y^1,
531 *P(nos-cas9, w+), M(3xP3-RFP.attP)ZH-2A, w**) (Port et al., 2014). An alanine was added before
532 the V5 tag (dashed underline) to prevent the creation of a potential tyrosine phosphorylation
533 site. Embryo injections were performed by BestGene (Chino Hills, CA, USA). Single F_0 flies were
534 crossed over the *TM6C*(*Sb*) balancer to establish stable lines. DNA was then extracted from
535 three flies of each of these independent lines, and V5 insertion events were detected by dot
536 blot using a mouse anti-V5 tag monoclonal antibody (Thermo Fisher Scientific, Ref. R960-25).
537 Positive strains were outcrossed in a w^{1118} background and their genomic DNA was sequenced
538 to check for proper in-frame V5 integration in *VhaAC45L*. One of these equivalent $VhaAC45L^{V5}$
539 mutant line was selected for further studies.
540

541 **Immunohistochemistry**

542 Adult brains of 8-day-old females, or 3rd-instar larva CNS, were dissected in *Drosophila* Ringer's
543 solution or hemolymph-like saline solution (HL3) (70 mM NaCl, 5 mM KCl, 1.5 mM $CaCl_2$, 70 mM
544 $MgCl_2$, 10 mM $NaHCO_3$, 115 mM sucrose, 5 mM trehalose, 5 mM HEPES, with pH adjusted to
545 7.6), respectively, and fixed in 4% paraformaldehyde (Thermo Fischer Scientific) for one hour.
546 After three 20-min washes in PBS plus 0.5% Triton X-100 (PBT), brains were blocked in PBT + 2%
547 bovine serum albumin for two hours. They were then incubated in primary antibodies diluted in
548 blocking solution for 24 h at 4°C. The primary antibodies used were: mouse monoclonal anti-V5
549 (Thermo Fisher Scientific, ref. R960-25, 1:200) and rat anti-CadN (DSHB, ref.DN-Ex #8, 1:20).

550 Brains were then washed three times, for 20 min each, in PBT before being incubated in
551 secondary antibodies for 2 hours. Secondary antibodies used were: Alexa Fluor 488 anti-mouse
552 and Alexa Fluor 555 anti-rat (Fisher Scientific, ref.A11029 and ref. A21434 respectively), all
553 diluted at 1:1000. After two 20-min washes in PBT followed by two 20-min washes in PBS, brains
554 were mounted in Prolong Gold Antifade Mountant (Thermo Fisher Scientific, ref. P36930).
555 Imaged were acquired on a Nikon A1R confocal microscope.
556 For immunostaining of the larval muscles and neuromuscular junctions, the Alexa Fluor 488
557 Tyramide SuperBoost Kit (Thermo Fisher, ref. B40912) was used to increase the V5 signal that
558 was otherwise faint in this tissue. The working protocol was as recommended by the
559 manufacturer, with anti-V5 diluted to 1:100, then followed by classical immunostaining, as
560 described above, to co-stain for the nerve terminals with an anti-HRP antibody (Jackson
561 ImmunoResearch, ref. 323-005-021, 1:200).
562

563 **Longevity assay**

564 About 110 virgin females from each genotype were collected on their hatching day, and placed
565 in clean bottles, with no more than 25 flies per bottle. Flies were transferred in new clean
566 bottles, and survivors were counted every two days for 60 days.
567

568 **Co-immunoprecipitation**

569 About 200 heads from 8 day-old *VhaAC45L*^{V5} and *w*^{1118} flies were lysed using glass beads in 500
570 µL of ice-cold lysis buffer: 50 mM Tris-HCl pH 7.4, 2 mM EDTA, 150 mM NaCl, 0.5% (vol/vol)
571 IGEPAL CA-630 (Sigma-Aldrich, ref. I3021), 10% (vol/vol) glycerol, 1 mM PMSF protease inhibitor

572 (Sigma-Aldrich, ref. P-7626) and 1X cOmplete Mini Protease Inhibitor Cocktail (Roche, ref.
573 11836153001). Samples were left on ice, with occasional gentle agitation, for 30 min before
574 being centrifuged at 12,000 rpm (13,000 g) at 4°C for 10 min to remove insoluble material. 400
575 µL of the supernatants were then added to 50 µL of Anti-V5-tag mAb-Magnetic Beads (MBL
576 International, Woburn, MA, USA, ref. M167-11), that had been previously washed as
577 recommended by the manufacturer. Samples were incubated with gentle agitation at 4°C for 4
578 hours. The supernatants were removed using a magnetic rack, and beads were washed three
579 times with 500 µM of ice-cold lysis buffer before being resuspended in 10 µL of milliQ water.
580

581 **Mass spectrometry**

582 The MS/MS analysis was performed at the Proteomics facility of the Institut Jacques Monod
583 (Université de Paris, Paris, France). Briefly, proteins were directly digested on the beads by
584 trypsin (Promega, Madison, WI, USA) overnight at 37°C in a 25-mM NH_4HCO_3 buffer (0.2 µg
585 trypsin in 20 µL). The resulting peptides were desalted on a ZipTip µ-C18 Pipette Tips (Pierce
586 Biotechnology, Rockford, IL, USA). Eluates were analyzed using either an Orbitrap Fusion or an
587 Orbitrap Q-Exactive Plus, coupled respectively to a Nano-LC Proxeon 1200 or a Nano-LC Proxeon
588 1000, both equipped with an easy spray ion source (Thermo Fisher Scientific, Waltham, MA,
589 USA). Raw data were processed on Proteome Discoverer 2.4 with the mascot node (Mascot
590 version 2.5.1), with a maximum of 2 missed cleavages authorized, against the Swissprot/TrEMBL
591 protein database release 2019_12 for *Drosophila melanogaster*. The following post-translational
592 modifications were included as variable: Acetyl (Protein N-term), Oxidation (M),
593 Phosphorylation (STY). Peptide identifications were validated with a 1% FDR (false discovery

594 rate) threshold calculated with the Percolator algorithm. Label-free quantification was done in
595 TOP 3 abundance calculation mode with pairwise ratio-based calculation and t-test (background
596 based) hypothesis test. Only proteins identified in at least one group in two independent
597 experiments were kept in the analysis. Missing values were set to the minimum abundance of
598 the experiment. A more detailed description of the LC-MS/MS procedure is provided in the
599 Supplementary Information.
600

601 **VMAT-pHluorin experiments**

602 Third-instar larvae expressing VMAT-pHluorin with or without *VhaAC45L* RNAi in motor neurons
603 using the *OK371-Gal4* driver, were dissected to expose the body wall muscles in Ca^{2+}-free HL3
604 saline solution (70 mM NaCl, 5 mM KCl, 70 mM $MgCl_2$, 10 mM $NaHCO_3$, 115 mM sucrose, 5 mM
605 trehalose, 5 mM HEPES, pH 7.6). Two other solutions were used: an acidic Ca^{2+}-free HL3 saline
606 (pH 5.5) and a neutral HL3-NH_4Cl saline (pH 7.6), in which 50 mM NaCl was replaced by 50 mM
607 NH_4Cl. After dissection, larvae fillets were allowed to settle in Ca^{2+}-free HL3 saline for 10 min
608 before being scanned a first time directly in a drop of the solution using a Nikon A1R confocal
609 microscope. Ca^{2+}-free HL3 saline was then replaced either by the acidic Ca^{2+}-free HL3 saline for
610 low pH-induced quenching experiments, or by the HL3- NH_4Cl saline for pH gradient collapse
611 experiments. In both cases, larval fillets were rinsed three times with the modified solution, and
612 incubated for 3 min, before being scanned a second time, in a drop of modified solution.
613 Quantification was done on Z-projections (set to maximal intensity) of confocal stacks. Using the
614 Fiji software, a fixed threshold was applied to all images to get rid of the background and select
615 only synaptic areas. Percentage of area over the threshold was used as a measure of the signal

616 intensity and ratios of the values obtained in modified solutions over standard HL3, i.e. the
617 second scan over the first scan, were calculated for quantifications.
618

619 **Larval locomotion assays**

620 Larval locomotion was assessed on an in-house made version of the FIMtable system (Risse et
621 al., 2014). Third-instar larvae were collected and briefly rinsed in water to remove traces of
622 food, before being gently placed on the recording table precoated with a thin layer of 1.2% agar
623 gel. Only four larvae of the same genotype were recorded simultaneously, to avoid collisions
624 between animals, for a period of 2 min with a Basler ace acA2040-25gm camera at 12.5
625 frames/s. Larvae that burrowed themselves into the agar plate or escaped the arena before the
626 end of recording were excluded from the results. Tracking was done using the FIMtrack
627 software, as described in (Risse et al., 2014). The number of peristaltic waves was computed
628 from the variations in larval area. More precisely, the curves of area variation were first
629 smoothed with a Savitzky-Golay filter to get rid of unwanted noise, then the number of waves
630 was defined as the number of peaks on the curve (which was automatically computed by a
631 custom-made Python script). Stride size was then calculated as the distance travelled by the
632 larva divided by the number of peristaltic waves, while stride duration was defined as the
633 recording time (i.e. 120 seconds) divided by the number of peristaltic waves.
634

635 **Electrophysiological recording and quantal analysis**

636 Third-instar larvae expressing *VhaAC45L* RNAi in motor neurons using the *OK371-Gal4* driver,
637 and appropriate controls, were dissected to expose the body wall muscles, and the brain

638 removed, in Ca^{2+}-free HL3 saline solution (70 mM NaCl, 5 mM KCl, 70 mM $MgCl_2$, 10 mM
639 $NaHCO_3$, 115 mM sucrose, 5 mM trehalose, 5 mM HEPES, pH 7.6) (Stewart et al., 1994; Cattaert
640 and Birman, 2001). Spontaneous miniature EPSPs (mEPSPs) were recorded in the presence of
641 tetrodotoxin (TTX) 10^{-6}M, so that no spike could occur, from the ventral longitudinal abdominal
642 muscle 6 in segment A3. Quantal analysis was performed following the theoretical background
643 described in (Kuno, 1971) and (Castellucci and Kandel, 1974). Distribution histograms of mEPSP
644 size were built from each muscle fiber recording with a 0.01 mV bin size. These histograms
645 provided an estimate of the mean size of a unitary EPSP, since the peaks represent integer
646 multiples of the unitary size. A theoretical distribution was then computed by convolving a
647 binomial distribution, accounting for quantal content (number of quanta released), and a
648 Gaussian distribution, allowing for variations in size of individual quanta. A detailed description
649 of the mathematical treatment is provided in the Supplementary Information.
650
651 **Statistical Analysis**
652 Statistical analysis was performed with the GraphPad Prism 6 software. The paired Student's t-
653 test was used for comparison of two genotypes, while either paired or unpaired ANOVA, with
654 Dunnett's post-test for multiple comparisons, were used for three genotypes.
655
656
657 ## Acknowledgements
658 We thank Dr Philippe Marin for helpful advice about the quantitative analysis of mass
659 spectrometry experiments, Drs Hervé Tricoire and Elodie Martin for helpful suggestion on the

660 CRISPR/Cas9 mutagenesis, Pr David Krantz for providing the *UAS-VMAT-pHluorin* strain, Dr Hervé
661 Tricoire for the *pCFD3: U6:3-gRNA* plasmid, and Dr. Céline Petitgas and Manon Dobrigna for
662 participating in preliminary experiments during their student internships. This work was
663 supported by a grant from the Fondation de France (Subvention n° 0086407) to SB and recurrent
664 fundings to his lab from the ESPCI Paris and CNRS. AD, ARI and JS were recipient of PhD fellowships
665 from PSL University and Labex MemoLife, the Doctoral School 3C and the China Scholarship
666 Council, respectively.

667

668 **Competing interests**

669 No competing interest to declare.

670

671

672 **References**

673

674 Abbas, Y. M., Wu, D., Bueler, S. A., Robinson, C. V., & Rubinstein, J. L. (2020). Structure of
675 V-ATPase from the mammalian brain. *Science*, *367*(6483), 1240-1246.

676

677 Allan, A. K., Du, J., Davies, S. A., & Dow, J. A. (2005). Genome-wide survey of V-ATPase
678 genes in *Drosophila* reveals a conserved renal phenotype for lethal alleles. *Physiological*
679 *genomics*, *22*(2), 128-138.

680

681 Cannata Serio, M., Rujano, M. A., & Simons, M. (2018). Mutations in ATP6AP2 cause
682 autophagic liver disease in humans. *Autophagy*, *14*(6), 1088-1089.
683
684 Castellucci, V. F., & Kandel, E. R. (1974). A quantal analysis of the synaptic depression
685 underlying habituation of the gill-withdrawal reflex in Aplysia. *Proceedings of the National*
686 *Academy of Sciences*, *71*(12), 5004-5008.
687
688 Cattaert, D., & Birman, S. (2001). Blockade of the central generator of locomotor rhythm
689 by noncompetitive NMDA receptor antagonists in *Drosophila* larvae. *Journal of neurobiology*,
690 *48*(1), 58-73.
691
692 Chintapalli, V. R., Wang, J., & Dow, J. A. (2007). Using FlyAtlas to identify better
693 *Drosophila melanogaster* models of human disease. *Nature genetics*, *39*(6), 715-720.
694
695 Colacurcio, D. J., & Nixon, R. A. (2016). Disorders of lysosomal acidification—the
696 emerging role of v-ATPase in aging and neurodegenerative disease. *Ageing research reviews*, *32*,
697 75-88.
698
699 Collins, M. P., & Forgac, M. (2020). Regulation and function of V-ATPases in physiology
700 and disease. *Biochimica et Biophysica Acta (BBA)-Biomembranes*, 183341.
701

Daniels, R. W., Collins, C. A., Chen, K., Gelfand, M. V., Featherstone, D. E., & DiAntonio, A. (2006). A single vesicular glutamate transporter is sufficient to fill a synaptic vesicle. *Neuron*, *49*(1), 11-16.

Davie, K., Janssens, J., Koldere, D., De Waegeneer, M., Pech, U., Kreft, Ł., ... & Poovathingal, S. (2018). A single-cell transcriptome atlas of the aging *Drosophila* brain. *Cell*, *174*(4), 982-998.

Davies, S. A., Goodwin, S. F., Kelly, D. C., Wang, Z., Sözen, M. A., Kaiser, K., & Dow, J. A. (1996). Analysis and inactivation of vha55, the gene encoding the vacuolar ATPase B-subunit in *Drosophila melanogaster* reveals a larval lethal phenotype. *Journal of Biological Chemistry*, *271*(48), 30677-30684.

Del Castillo, J., & Katz, B. (1954). Quantal components of the end-plate potential. *The Journal of physiology*, *124*(3), 560.

Dietzl, G., Chen, D., Schnorrer, F., Su, K. C., Barinova, Y., Fellner, M., ... & Couto, A. (2007). A genome-wide transgenic RNAi library for conditional gene inactivation in *Drosophila*. *Nature*, *448*(7150), 151-156.

Dubos, A., Castells-Nobau, A., Meziane, H., Oortveld, M. A., Houbaert, X., Iacono, G., ... & Bhukel, A. (2015). Conditional depletion of intellectual disability and Parkinsonism candidate

724 gene ATP6AP2 in fly and mouse induces cognitive impairment and neurodegeneration. *Human*
725 *molecular genetics*, *24*(23), 6736-6755.
726
727 Forgac, M. (2007). Vacuolar ATPases: rotary proton pumps in physiology and
728 pathophysiology. *Nature reviews Molecular cell biology*, *8*(11), 917-929.
729
730 Goh, G. Y., Huang, H., Ullman, J., Borre, L., Hnasko, T. S., Trussell, L. O., & Edwards, R. H.
731 (2011). Presynaptic regulation of quantal size: K+/H+ exchange stimulates vesicular glutamate
732 transport. *Nature neuroscience*, *14*(10), 1285-1292.
733
734 Gowrisankaran, S., & Milosevic, I. (2020). Regulation of synaptic vesicle acidification at
735 the neuronal synapse. *IUBMB life*, *72*(4), 568-576.
736
737 Guida, M. C., Hermle, T., Graham, L. A., Hauser, V., Ryan, M., Stevens, T. H., & Simons, M.
738 (2018). ATP6AP2 functions as a V-ATPase assembly factor in the endoplasmic reticulum.
739 *Molecular biology of the cell*, *29*(18), 2156-2164.
740
741 Hiesinger, P. R., Fayyazuddin, A., Mehta, S. Q., Rosenmund, T., Schulze, K. L., Zhai, R. G.,
742 ... & Bellen, H. J. (2005). The v-ATPase V0 subunit a1 is required for a late step in synaptic vesicle
743 exocytosis in *Drosophila*. *Cell*, *121*(4), 607-620.
744

745 Huang, H., & Trussell, L. O. (2014). Presynaptic HCN channels regulate vesicular
746 glutamate transport. *Neuron*, *84*(2), 340-346.
747
748 Ichihara, A., & Yatabe, M. S. (2019). The (pro) renin receptor in health and disease.
749 *Nature Reviews Nephrology*, 1.
750
751 Inoue, H., Noumi, T., Nagata, M., Murakami, H., & Kanazawa, H. (1999). Targeted
752 disruption of the gene encoding the proteolipid subunit of mouse vacuolar H+-ATPase leads to
753 early embryonic lethality. *Biochimica et Biophysica Acta (BBA)-Bioenergetics*, *1413*(3), 130-138.
754
755 Jan, L. Y. & Jan, Y. N. (1982). Antibodies to horseradish peroxidase as specific neuronal
756 markers in *Drosophila* and in grasshopper embryos. *Proceedings of the National Academy of*
757 *Sciences USA*, 79(8), 2700-2704
758
759 Jansen, E. J. R., & Martens, G. J. M. (2012). Novel insights into V-ATPase functioning:
760 distinct roles for its accessory subunits ATP6AP1/Ac45 and ATP6AP2/(pro) renin receptor.
761 *Current Protein and Peptide Science*, *13*(2), 124-133.
762
763 Jansen, E. J., Timal, S., Ryan, M., Ashikov, A., Van Scherpenzeel, M., Graham, L. A., ... &
764 Steenbergen, G. (2016). ATP6AP1 deficiency causes an immunodeficiency with hepatopathy,
765 cognitive impairment and abnormal protein glycosylation. *Nature communications*, *7*(1), 1-13.
766

767 Korvatska, O., Strand, N. S., Berndt, J. D., Strovas, T., Chen, D. H., Leverenz, J. B., ... &
768 Bonkowski, E. (2013). Altered splicing of ATP6AP2 causes X-linked parkinsonism with spasticity
769 (XPDS). *Human molecular genetics*, *22*(16), 3259-3268.
770
771 Kuno, M. (1971). Quantum aspects of central and ganglionic synaptic transmission in
772 vertebrates. *Physiological Reviews*, *51*(4), 647-678.
773
774 Lee, S. K., Li, W., Ryu, S. E., Rhim, T., & Ahnn, J. (2010). Vacuolar (H+)-ATPases in
775 Caenorhabditis elegans: what can we learn about giant H+ pumps from tiny worms?. *Biochimica*
776 *et Biophysica Acta (BBA)-Bioenergetics*, *1797*(10), 1687-1695.
777
778 Lin, D. M., & Goodman, C. S. (1994). Ectopic and increased expression of Fasciclin II alters
779 motoneuron growth cone guidance. *Neuron*, *13*(3), 507-523.
780
781 Mahr, A., & Aberle, H. (2006). The expression pattern of the *Drosophila* vesicular
782 glutamate transporter: a marker protein for motoneurons and glutamatergic centers in the
783 brain. *Gene Expression Patterns*, *6*(3), 299-309.
784
785 Manolson, M. F., Wu, B., Proteau, D., Taillon, B. E., Roberts, B. T., Hoyt, M. A., & Jones, E.
786 W. (1994). STV1 gene encodes functional homologue of 95-kDa yeast vacuolar H (+)-ATPase
787 subunit Vph1p. *Journal of Biological Chemistry*, *269*(19), 14064-14074.
788

789 Maycox, P. R., Deckwerth, T., Hell, J. W., & Jahn, R. (1988). Glutamate uptake by brain
790 synaptic vesicles. Energy dependence of transport and functional reconstitution in
791 proteoliposomes. *Journal of Biological Chemistry*, *263*(30), 15423-15428.
792
793 Miesenböck, G., De Angelis, D. A., & Rothman, J. E. (1998). Visualizing secretion and
794 synaptic transmission with pH-sensitive green fluorescent proteins. *Nature*, *394*(6689), 192-195.
795
796 Mitchell, A. L., Attwood, T. K., Babbitt, P. C., Blum, M., Bork, P., Bridge, A., ... & Gough, J.
797 (2019). InterPro in 2019: improving coverage, classification and access to protein sequence
798 annotations. *Nucleic acids research*, *47*(D1), D351-D360.
799
800 Morel, N., Gérard, V., & Shiff, G. (1998). Vacuolar H+-ATPase domains are transported
801 separately in axons and assemble in *Torpedo* nerve endings. *Journal of neurochemistry*, *71*(4),
802 1702-1708.
803
804 Morel, N., Dedieu, J. C., & Philippe, J. M. (2003). Specific sorting of the a1 isoform of the
805 V-H+ ATPase a subunit to nerve terminals where it associates with both synaptic vesicles and
806 the presynaptic plasma membrane. *Journal of Cell Science*, *116*(23), 4751-4762.
807
808 Moriyama, Y., Maeda, M., & Futai, M. (1992). The role of V-ATPase in neuronal and
809 endocrine systems. *Journal of Experimental Biology*, *172*(1), 171-178.
810

811 Nagarkar-Jaiswal, S., Lee, P. T., Campbell, M. E., Chen, K., Anguiano-Zarate, S., Gutierrez,
812 M. C., ... & Booth, B. W. (2015). A library of MiMICs allows tagging of genes and reversible,
813 spatial and temporal knockdown of proteins in *Drosophila*. *Elife*, *4*, e05338.
814
815 Nelson, N. (2003). A journey from mammals to yeast with vacuolar H+-ATPase (V-
816 ATPase). *Journal of bioenergetics and biomembranes*, *35*(4), 281-289.
817
818 Nguyen, G. (2010). The (pro) renin receptor in health and disease. *Annals of medicine*,
819 *42*(1), 13-18.
820
821 Parks, A. L., Cook, K. R., Belvin, M., Dompe, N. A., Fawcett, R., Huppert, K., ... & Deal-
822 Herr, M. E. (2004). Systematic generation of high-resolution deletion coverage of the *Drosophila*
823 *melanogaster* genome. *Nature genetics*, *36*(3), 288-292.
824
825 Perkins, L. A., Holderbaum, L., Tao, R., Hu, Y., Sopko, R., McCall, K., ... & Miller, A. (2015).
826 The transgenic RNAi project at Harvard Medical School: resources and validation. *Genetics*,
827 *201*(3), 843-852.
828
829 Port, F., Chen, H. M., Lee, T., & Bullock, S. L. (2014). Optimized CRISPR/Cas tools for
830 efficient germline and somatic genome engineering in *Drosophila*. *Proceedings of the National*
831 *Academy of Sciences*, *111*(29), E2967-E2976.
832

833 Poskanzer, K. E., & Davis, G. W. (2004). Mobilization and fusion of a non-recycling pool of
834 synaptic vesicles under conditions of endocytic blockade. *Neuropharmacology*, *47*(5), 714-723.
835
836 Risse, B., Otto, N., Berh, D., Jiang, X., & Klämbt, C. (2014). FIM imaging and FIMtrack: two
837 new tools allowing high-throughput and cost effective locomotion analysis. *JoVE (Journal of*
838 *Visualized Experiments)*, (94), e52207.
839
840 Saroussi, S., & Nelson, N. (2009). The little we know on the structure and machinery of V-
841 ATPase. *Journal of Experimental Biology*, *212*(11), 1604-1610.
842
843 Sautin, Y. Y., Lu, M., Gaugler, A., Zhang, L., & Gluck, S. L. (2005). Phosphatidylinositol 3-
844 kinase-mediated effects of glucose on vacuolar H+-ATPase assembly, translocation, and
845 acidification of intracellular compartments in renal epithelial cells. *Molecular and cellular*
846 *biology*, *25*(2), 575-589.
847
848 Schoonderwoert, V. T. G., & Martens, G. J. (2002-a). Structural gene organization and
849 evolutionary aspects of the V-ATPase accessory subunit Ac45. *Biochimica et Biophysica Acta*
850 *(BBA)-Gene Structure and Expression*, *1574*(3), 245-254.
851
852 Schoonderwoert, V. T. G., & Martens, G. J. (2002-b). Targeted disruption of the mouse
853 gene encoding the V-ATPase accessory subunit Ac45. *Molecular membrane biology*, *19*(1), 67-
854 71.

855

856 Shao, E., & Forgac, M. (2004). Involvement of the nonhomologous region of subunit A of
857 the yeast V-ATPase in coupling and in vivo dissociation. *Journal of Biological Chemistry*, *279*(47),
858 48663-48670.

859

860 Stewart, B. A., Atwood, H. L., Renger, J. J., Wang, J., & Wu, C. F. (1994). Improved stability
861 of *Drosophila* larval neuromuscular preparations in haemolymph-like physiological solutions.
862 *Journal of Comparative Physiology A*, *175*(2), 179-191.

863

864 Tabb, J. S., Kish, P. E., Van Dyke, R., & Ueda, T. (1992). Glutamate transport into synaptic
865 vesicles. Roles of membrane potential, pH gradient, and intravesicular pH. *Journal of Biological*
866 *Chemistry*, *267*(22), 15412-15418.

867

868 Takamori, S. (2016). Presynaptic molecular determinants of quantal size. *Frontiers in*
869 *synaptic neuroscience*, *8*, 2.

870

871 Thurmond, J., Goodman, J. L., Strelets, V. B., Attrill, H., Gramates, L. S., Marygold, S. J., ...
872 & Kaufman, T. C. (2019). FlyBase 2.0: the next generation. *Nucleic acids research*, *47*(D1), D759-
873 D765.

874

875 Vasanthakumar, T., & Rubinstein, J. L. (2020). Structure and Roles of V-type ATPases.
876 *Trends in Biochemical Sciences*, *45*(4), 295-307.

877

878 Voss, M., Vitavska, O., Walz, B., Wieczorek, H., & Baumann, O. (2007). Stimulus-induced
879 phosphorylation of vacuolar H+-ATPase by protein kinase A. *Journal of Biological Chemistry*,
880 *282*(46), 33735-33742.

881

882 Wu, T. H., Lu, Y. N., Chuang, C. L., Wu, C. L., Chiang, A. S., Krantz, D. E., & Chang, H. Y.
883 (2013). Loss of vesicular dopamine release precedes tauopathy in degenerative dopaminergic
884 neurons in a *Drosophila* model expressing human tau. *Acta neuropathologica*, *125*(5), 711-725.

885

886 # A novel and specific regulator of neuronal V-ATPase in *Drosophila*

887

888 Amina Dulac, Abdul-Raouf Issa, Jun Sun, Giorgio Matassi, Baya Chérif-Zahar, Daniel

889 Cattaert and Serge Birman

890

891 ## Supplementary information

892

893 **Supplementary figures**

894 **Supplementary tables**

895 **Supplementary methods**

896

897

898 **Supplementary figures**

899

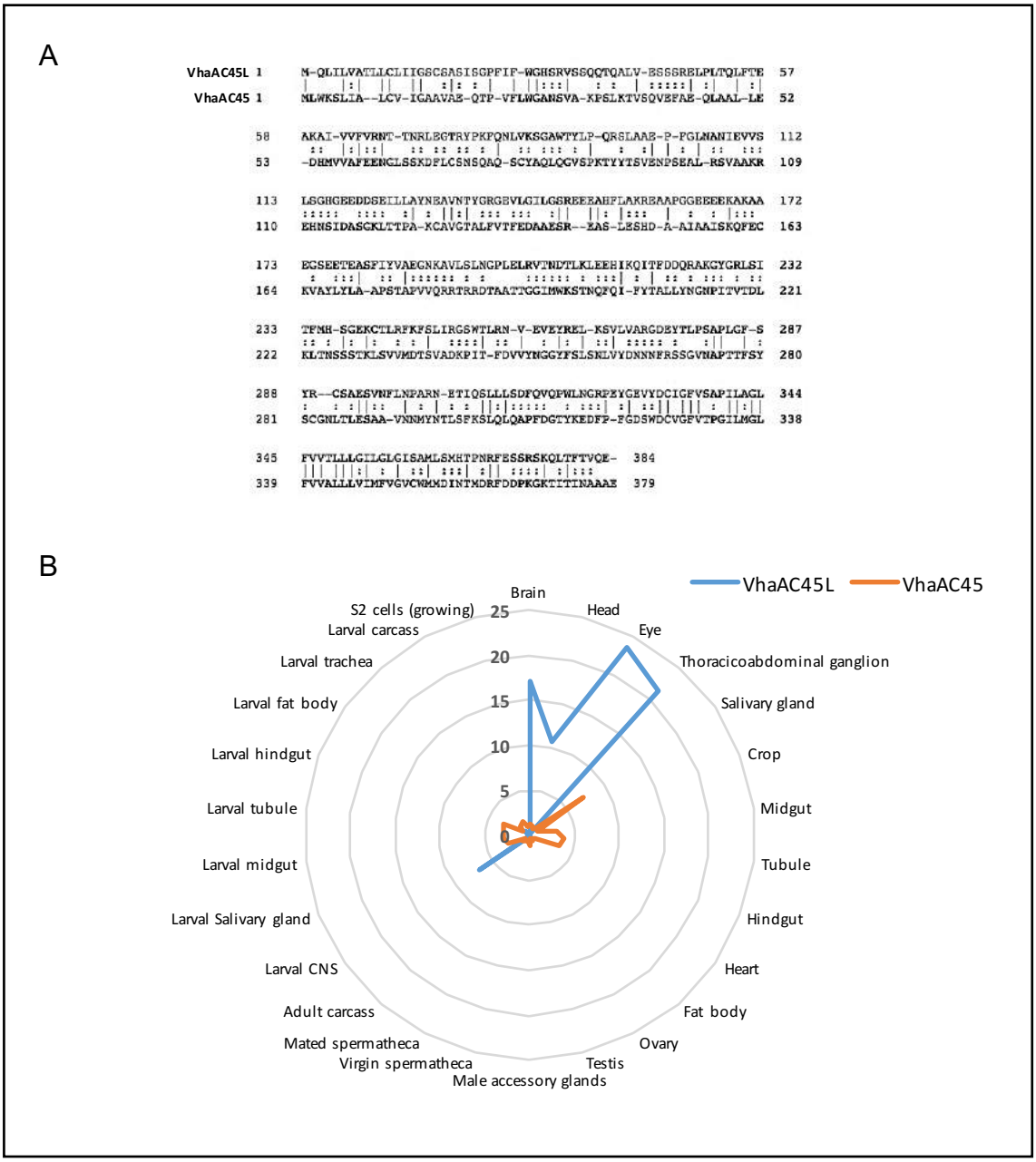

900

901 **Supplementary Figure 1.** *VhaAC45L* is a paralog of *VhaAC45* expressed in the nervous system. (**A**) Amino-

902 acid sequence alignment shows that VhaAC45L and VhaAC45 share 69.9% similarity. (B) Diagram

903 representing expression levels of *VhaAC45L* and *VhaAC45* in different tissues relative to the whole fly,

904 according to FlyAtlas data (Chintapalli et al., 2007). VhaAC45L appears to be markedly enriched in the
905 nervous system of larva and adult fly, whereas in contrast VhaAC45 seems to be uniformly expressed in
906 all tissues in these two stages.
907
908

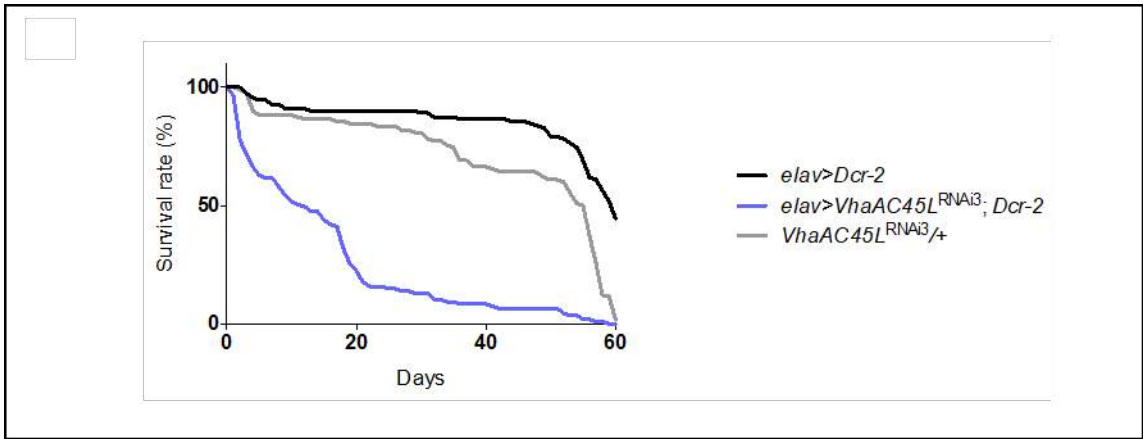

909

910 **Supplementary Figure 2.** Knockdown of *VhaAC45L* expression in neurons decreases adult longevity. Pan-
911 neuronal expression of *VhaAC45L*^{RNAi3} and *Dcr-2* with the *elav-Gal4* driver led to a marked shortening of
912 the lifespan of adult flies. Results of one experiment, carried out with 105-110 females per genotype.
913
914
915
916
917
918
919

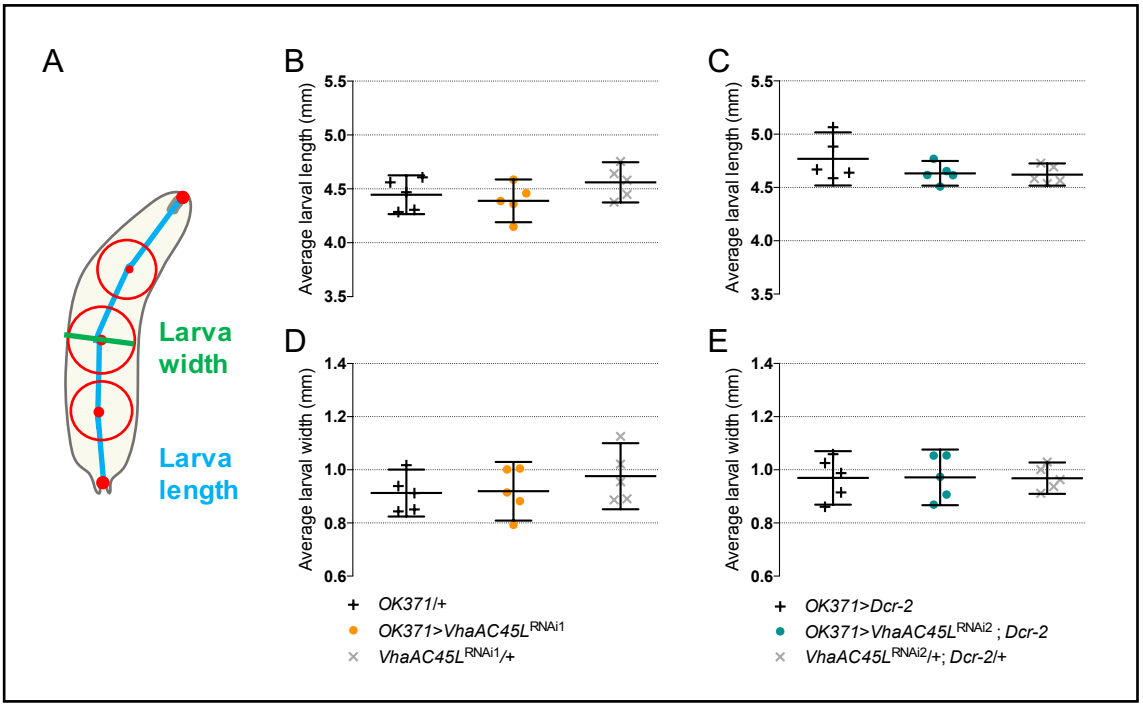

920

921 **Supplementary Figure 3.** VhaAC45L downregulation in motoneurons did not significantly alter larval size.

922 (**A**) Larval length is defined as the spine length from head to tail, while larval width is the diameter of the

923 mid-spine circle. (**B-E**) Average larval length (**B**, **C**) and width (**D**, **E**) were not significantly different

924 between animals expressing *VhaAC45L* RNAi in motoneurons and controls.

925

926

927

928

929

930 ## Supplementary tables

931

932 **Supplementary Table 1.** Pan-neuronal expression of *VhaAC45L* rescues the embryonic lethality of

933 VhaAC45L-deficient flies up to the adult stage.

Genotype of the progeny flies[1]	**Expected percentage**[2]	**Scored percentage**[3]
Heterozygous deficiency without *VhaAC45L* expression	40	39.7
Heterozygous deficiency with pan-neuronal *VhaAC45L* expression	40	53.8
Homozygous deficiency without *VhaAC45L* expression	0	0
Homozygous deficiency with pan-neuronal *VhaAC45L* expression	20	6.4

934 [1]Rescue of embryonic lethality was assayed by crossing *elav-Gal4*; *VhaAC45L*^{MI107}/*TM6B*(*Tb*) females with *w*;

935 *UAS-VhaAC45L*/*CyO*; *Df(3R)Exel6214*/*TM6B*(*Tb*) males, and scoring the relative number of VhaAC45L-

936 expressing adult flies homozygous for *VhaAC45L* deficiency (i.e. non-*Tb* and non-*Cy elav-Gal4/+*; *UAS-*

937 *VhaAC45L/+*; *VhaAC45L*^{MI107}/*Df(3R)Exel6214*) in the progeny (highlighted line).

938 [2]Expected percentage of adult progeny flies of each genotype in case of full rescue.

939 [3]Actual percentage obtained in the experiments. 24 rescued adults were recovered out of a total of 373

940 progeny flies.

941

942

943

944

945

946

947 **Supplementary Table 2.** List of the genes encoding proteins that co-immunoprecipitated with VhaAC45L

948 in *Drosophila* head extracts.

Gene Symbol[1]	FlyBase Gene ID	$Log_2(R_1)$	$Log_2(R_2)$	$Log_2(R_3)$
ATP6AP2	FBgn0037671	6.154281057	9.481786693	5.17436482
Vha100-1	FBgn0028671	1.499248537	8.012982519	5.43599503
VhaAC39-1	FBgn0028665	2.104797507	8.293264658	4.86741949
VhaAC45L	FBgn0051030	3.669278876	7.960835791	5,19465574
Twdlβ	FBgn0033658	1.642952792	3.068640973	2.35207192
Ccp84Ag	FBgn0004777	1.543972087	1.326485589	1.86392045
CG13627	FBgn0039217	5.738384187	4.008318188	3.18433108
mfas	FBgn0260745	1.596554441	3.368384477	3.03376685
CG16820	FBgn0032495	4.77051909	9.784086057	3.60280541
Cpr64Ab	FBgn0035511	1.08994458	2.758609792	2.31103817
CG14752	FBgn0033307	2.21698759	3.69458382	3.10154816
CG15615	FBgn0034159	2.77101281	5.12362053	3.39808341

949

950 [1]12 proteins were identified with at least twice higher abundance in *VhaAC45L*^{V5} compared to the *w*^{1118}

951 control in three independent co-immunoprecipitations with anti-V5 antibodies, followed by mass-

952 spectrometry analysis experiments. Among these proteins, three are known to be constitutive or

953 accessory subunits of the V-ATPase complex. They are indicated in the first ochre-highlighted lines of the

954 Table and circled in blue in Fig. 2. The grey line indicates the co-immunoprecipitation target VhaAC45L.

955

956

957

958

959 **Supplementary Table 3.** *Drosophila* strains used in this study.
960

Names	***Genotypes***	***Usage***	***Sources***	***References***
w^{1118}	*w*^{1118}	Wild-type control line	In-house collection	Hazelrigg et al. 1984
UAS-VhaAC45L	w; P*{w*$^{+mW.hs}$*=CG31030*^{UAS}*}; +*	Expression of *Drosophila VhaAC45L*	In-house construct	This report
VhaAC45L^{V5}	*w; CG31030*^{V5}	Insertion of a V5 tag in *VhaAC45L*	In-house construct	This report
VhaAC45L^{RNAi1}	*y, sc, v, sev*^{21}*; P{y*$^{+t7.7}$ *v*$^{+t1.8}$*=TRiP.HMC05568}attP40*	*VhaAC45L* knock down	BDSC line n°64549	Perkins *et al.*, 2015
VhaAC45L^{RNAi2}	*y, w*^{1118} *; P{KK106825}VIE-260B*	*VhaAC45L* knock down	VDRC n°107398	Dietzl *et al.*, 2007
VhaAC45L^{RNAi3}	*w*^{1118}*; P{GD381}v33095*/TM3	*VhaAC45L* knock down	VDRC n°33095	Dietzl *et al.*, 2007
VhaAC45L^{MI107}	*y, w; Mi{y*$^{+mDint2}$*=MIC}CG31030*^{MI00107} */TM3, Sb, Ser*	MIMIC *VhaAC45L* mutant	BDSC line n°30620	Nagarkar-Jaiswal *et al.*, 2015
Df(3R)Exel6214	*w*^{1118}*; Df(3R)Exel6214, P{w*$^{+mC}$*=XP-U}Exel6214/TM6B, Tb*	Deficiency covering *VhaAC45L* and ~20 other genes	BDSC line n°7692	Parks *et al.*, 2004
elav-Gal4	*P{w*$^{+mW.hs}$*=GawB}elav*^{C155}	Pan-neuronal driver	BDSC line n°458	Lin and Goodman, 1994
OK371-Gal4	*w*^{1118}*; P{w*$^{+mW.hs}$*=GawB}VGlut*^{OK371}	Glutamatergic and motor neuron driver	Gift of Hermann Aberle, Heinrich Heine University, Düsseldorf, Germany	Mahr and Aberle, 2006
UAS-VMAT-pHluorin	*w; Vmat*$^{UAS.pHluorin}$	Expression of *Drosophila* Vmat fused to the pH-sensitive fluorescent marker ecliptic pHluorin	Gift of David Krantz,UCLA, Los Angeles, USA	Wu *et al.*, 2013

961
962

963 **Supplementary methods**

964

965 **Detailed LC-MS/MS procedure**

966 Proteins on beads were digested overnight at 37°C with trypsin (Promega, Madison, WI, USA) in
967 25 mM NH_4HCO_3 buffer (0.2 µg trypsin in 20 µL). The resulting peptides were desalted using
968 ZipTip µ-C18 Pipette Tips (Pierce Biotechnology, Rockford, IL, USA). Samples were analyzed
969 using either an Orbitrap Fusion or an Orbitrap Q-Exactive Plus, coupled respectively to a Nano-
970 LC Proxeon 1200 or a Nano-LC Proxeon 1000, both equipped with an easy spray ion source
971 (Thermo Fisher Scientific, Waltham, MA, USA). On the Orbitrap Fusion instrument, peptides
972 were loaded with an online preconcentration method and separated by chromatography using a
973 Pepmap-RSLC C18 column (0.75 x 750 mm, 2 µm, 100 Å) from Thermo Fisher Scientific,
974 equilibrated at 50°C and operated at a flow rate of 300 nl/min. Peptides were eluted by a
975 gradient of solvent A (H_2O, 0.1 % FA) and solvent B (ACN/H_2O 80/20, 0.1% FA). The column was
976 first equilibrated for 5 min with 95 % of A, then B was raised to 28 % in 105 min and to 40% in
977 15 min. Finally, the column was washed with 95% B during 20 min and re-equilibrated at 95% A
978 for 10 min. Peptides masses were analyzed in the Orbitrap cell in full ion scan mode, at a
979 resolution of 120,000, a mass range of *m/z* 350-1550 and an AGC target of 4.10^5. MS/MS were
980 performed in the top speed 3s mode. Peptides were selected for fragmentation by Higher-
981 energy C-trap Dissociation (HCD) with a Normalized Collisional Energy of 27% and a dynamic
982 exclusion of 60 seconds. Fragment masses were measured in an Ion trap in the rapid mode, with
983 and an AGC target of 1.10^4. Monocharged peptides and unassigned charge states were excluded

984 from the MS/MS acquisition. The maximum ion accumulation times were set to 100 ms for MS
985 and 35 ms for MS/MS acquisitions respectively.
986 On the Q-Exactive Plus instrument, peptides were loaded with an online preconcentration
987 method and separated by chromatography using a Pepmap-RSLC C18 column (0.75 x 500 mm, 2
988 µm, 100 Å) from Thermo Scientific, equilibrated at 50°C and operated at a flow rate of 300
989 nl/min. Peptides were eluted by a gradient of solvent A (H_2O, 0.1 % FA) and solvent B (100 %
990 ACN, 0.1% FA), the column was first equilibrated 5 min with 95 % of A, then B was raised to 35
991 % in 93 min and finally, the column was washed with 80% B during 10 min and re-equilibrated at
992 95% A during 10 min. Peptides masses were analyzed in the Orbitrap cell in full ion scan mode
993 at a resolution of 70,000 with a mass range of *m/z* 375-1500 and an AGC target of 3.10^6. MS/MS
994 were performed in a Top 20 DDA mode. Peptides were selected for fragmentation by Higher-
995 energy C-trap Dissociation (HCD) with a Normalized Collisional Energy of 27%, and a dynamic
996 exclusion of 30 seconds. Fragment masses were measured in the Orbitrap cell at a resolution of
997 17,500, with an AGC target of 2.10^5. Monocharged peptides and unassigned charge states were
998 excluded from the MS/MS acquisition. The maximum ion accumulation times were set to 50 ms
999 for MS and 45 ms for MS/MS acquisitions respectively.
1000
1001 Raw data were processed on Proteome Discoverer 2.4 with the mascot node (Mascot version
1002 2.5.1), with the Swissprot/TrEMBL protein database release 2019_12 for *Drosophila*
1003 *melanogaster*. A maximum of 2 missed cleavages was authorized. Precursor and fragment mass
1004 tolerances were set to respectively 7 ppm and 0.5 Da (Orbitrap Fusion) and to 6 ppm and 0.02
1005 Da (Orbitrap Q-exactive Plus). The following post-translational modifications were included as

1006 variable: Acetyl (Protein N-term), Oxidation (M), Phosphorylation (STY). Spectra were filtered
1007 using a 1% FDR (false discovery rate) with the percolator node. Label-free quantification was
1008 done in TOP 3 abundance calculation mode with pairwise ratio based calculation and t-test
1009 (background based) hypothesis test.
1010

1011 **Quantal analysis**

1012 The probability for an EPSP to contain i quanta followed a binomial distribution:

1013 $$\mathrm{P}(i) = \mathrm{C}_n^i \times p^i \times (1-p)^{(n-i)} \qquad (1)$$

1014 in which p is the average probability of release, and n is the total number of releasable quanta.
1015 In the frequency distribution of EPSP amplitude, successive peaks represent increasing numbers
1016 of quanta.
1017 In order to predict how these events are distributed between different bins in a histogram, it is
1018 necessary to allow for variations in quantal size. To do this, the largest peaks of the histogram
1019 were fitted to a Gaussian curve scaled in width to have a variance proportional to quantal size,
1020 and scaled in height so that its area corresponded to the predicted number of events (Del
1021 Castillo and Katz, 1954). From the mean (μ) and standard deviation (σ) of the Gaussian curve,
1022 the content (f) of each bin (y) is given by:

1023 $$f(y) = \frac{1}{\sqrt{2\pi}\sigma} e^{-\frac{1}{2}\left(\frac{y-\mu}{\sigma}\right)^2} \qquad (2)$$

1024 The standard deviation (σ) of each peak depends on the number of quanta it contains. It was
1025 calculated as follows:

1026 $$\sigma = i \times \sqrt{\sigma_0} \qquad (3)$$

with i the number of quanta in the peak, and σ_0 the standard deviation of a single quanta. The amplitude of Gaussian distribution for each peak is scaled to the probability $P(i)$ for that peak (see *(1)*).

The complete theoretical distribution, allowing for variance and peak overlap was then obtained by pooling the Gaussians for all peaks. In this way, the theoretical distribution could be superimposed on the histogram for direct comparison with the data.